NUCLEAR DATA AND MEASUREMENTS SERIES

ANL/NDM-114

Ambiguities in the Elastic Scattering of 8 MeV Neutrons from Adjacent Nuclei

by

A.B. Smith, R.D. Lawson, and P.T. Guenther

October 1989

ARGONNE NATIONAL LABORATORY,
ARGONNE, ILLINOIS 60439, U.S.A.

NUCLEAR DATA AND MEASUREMENTS SERIES

ANL/NDM–114

AMBIGUITIES IN THE ELASTIC SCATTERING OF 8 MeV NEUTRONS FROM ADJACENT NUCLEI

A. B. Smith, R. D. Lawson, and P. T. Guenther

October 1989

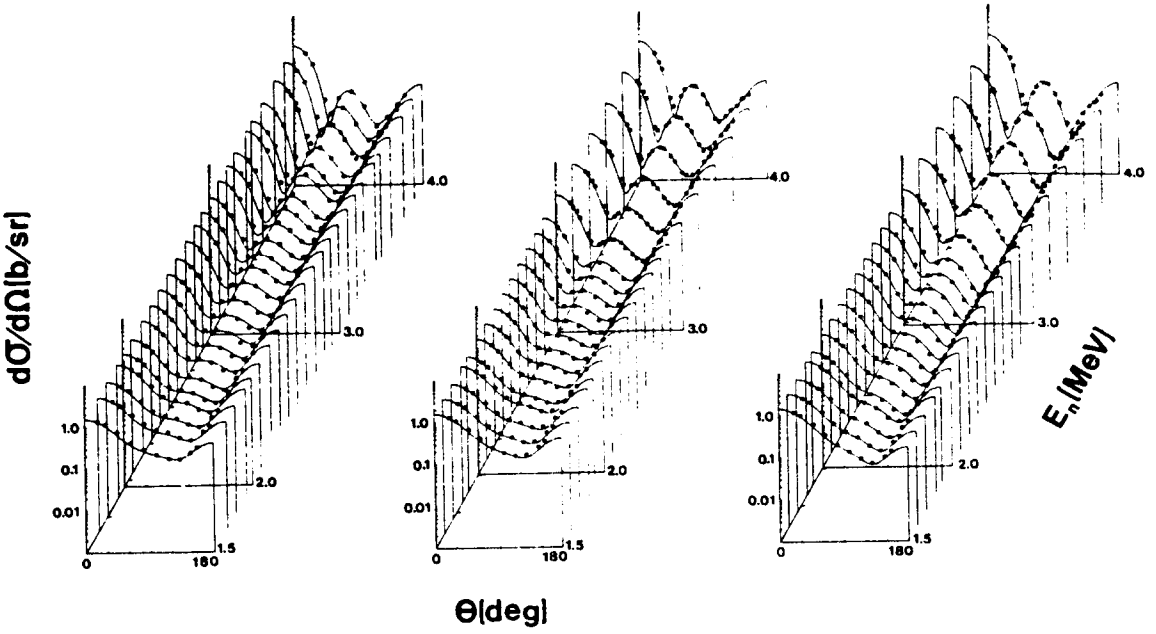

ARGONNE NATIONAL LABORATORY, ARGONNE, ILLINOIS

Operated by THE UNIVERSITY OF CHICAGO

for the U. S. DEPARTMENT OF ENERGY

under Contract W-31-109-Eng-38

This report has been reproduced from the best available copy.

Available from the
National Technical Information Service
U.S. Department of Commerce
5285 Port Royal Road
Springfield, VA 22161

Price: Printed Copy A03
Microfiche A01

ANL/NDM–114

AMBIGUITIES IN THE ELASTIC SCATTERING OF 8 MeV NEUTRONS FROM ADJACENT NUCLEI*

by

A. B. Smith, R. D. Lawson, and P. T. Guenther

October 1989

Keywords

Measured $d\sigma/d\Omega$ ratios for elastic–scattering of 8.0 MeV neutrons. Model discussion.

Engineering Physics Division
ARGONNE NATIONAL LABORATORY
9700 South Cass Avenue
Argonne, Illinois 60439
U. S. A.

*This work supported by the United States Department of Energy under contract W–31–109–Eng–38.

NUCLEAR DATA AND MEASUREMENTS SERIES

The Nuclear Data and Measurements Series presents results of studies in the field of microscopic nuclear data. The primary objective is the dissemination of information in the comprehensive form required for nuclear technology applications. This Series is devoted to: a) measured microscopic nuclear parameters, b) experimental techniques and facilities employed in measurements, c) the analysis, correlation and interpretation of nuclear data, and d) the evaluation of nuclear data. Contributions to this Series are reviewed to assure technical competence and, unless otherwise stated, the contents can be formally referenced. This Series does not supplant formal journal publication, but it does provide the more extensive information required for technological applications (e.g., tabulated numerical data) in a timely manner.

TABLE OF CONTENTS

INFORMATION ABOUT OTHER ISSUES OF THE ANL/NDM SERIES

A list of titles and authors for all the previous issues appears in each report of the series. The list for reports ANL/NDM–1 through ANL/NDM–75 appears in ANL/NDM–76, and ANL/NDM–91 contains the list for reports ANL/NDM–76 through ANL/NDM–90. Below is the list for ANL/NDM–91 up to the current report. Requests for a complete list of titles or for copies of previous reports should be directed to:

Section Secretary
Applied Nuclear Physics Section
Engineering Physics Division
Building 316
Argonne National Laboratory
9700 South Cass Avenue
Argonne, Illinois 60439
U.S.A.

ANL/NDM–91 A.B. Smith, P.T. Guenther and R.D. Lawson, *On the Energy Dependence of the Optical Model of Neutron Scattering from Niobium*, May 1985.

ANL/NDM–92 Donald L. Smith, *Nuclear Data Uncertainties (Vol.–I): Basic Concepts of Probability*, December 1988.

ANL/NDM–93 D.L. Smith, J.W. Meadows and M.M. Bretscher, *Integral Cross–section Measurements for $^{7}Li(n,n't)^{4}He$, $^{27}Al(n,p)^{27}Mg$, $^{27}Al(n,\alpha)^{24}Na$, $^{58}Ni(n,p)^{58}Co$, and $^{60}Ni(n,p)^{60}Co$ Relative to ^{238}U Neutron Fission in the Thick–target $^{9}Be(d,n)^{10}B$ Spectrum at $E_d = 7$ MeV*, October 1985.

ANL/NDM–94 A.B. Smith, D.L. Smith, P. Rousset, R.D. Lawson and R.J. Howerton, *Evaluated Neutronic Data File for Yttrium*, January 1986.

ANL/NDM–95 Donald L. Smith and James W. Meadows, *A Facility for High–intensity Neutron Irradiations Using Thick–target Sources at the Argonne Fast–neutron Generator*, May 1986.

ANL/NDM–96 M. Sugimoto, A.B. Smith and P.T. Guenther, *Ratio of the Prompt–fission–neutron Spectrum of Plutonium–239 to that of Uranium–235*, September 1986.

ANL/NDM–97 J.W. Meadows, *The Fission Cross Sections of ^{230}Th, ^{232}Th, ^{233}U, ^{234}U, ^{236}U, ^{238}U, ^{237}Np, ^{239}Pu, and ^{242}Pu Relative ^{235}U at 14.74 MeV Neutron Energy*, December 1986.

ANL/NDM–98 J.W. Meadows, *The Fission Cross Section Ratios and Error Analysis for Ten Thorium, Uranium, Neptunium and Plutonium Isotopes at 14.74–MeV Neutron Energy*, March 1987.

ANL/NDM–99 Donald L. Smith, *Some Comments on the Effects of Long–range Correlations in Covariance Matrices for Nuclear Data*, March 1987.

ANL/NDM–100 A.B. Smith, P.T. Guenther and R.D. Lawson, *The Energy Dependence of the Optical–model Potential for Fast–neutron Scattering from Bismuth*, May 1987.

ANL/NDM–101 A.B. Smith, P.T. Guenther, J.F. Whalen and R.D. Lawson, *Cobalt: Fast Neutrons and Physical Models*, July 1987.

ANL/NDM–102 D. L Smith, *Investigation of the Influence of the Neutron Spectrum in Determinations of Integral Neutron Cross–Section Ratios*, November 1987.

ANL/NDM–103 A.B. Smith, P.T. Guenther and B. Micklich, *Spectrum of Neutrons Emitted From a Thick Beryllium Target Bombarded With 7 MeV Deuterons*, January 1988.

ANL/NDM–104 L.P. Geraldo and D.L. Smith, *Some Thoughts on Positive Definiteness in the Consideration of Nuclear Data Covariance Matrices*, January 1988.

ANL/NDM–105 A.B. Smith, D.L. Smith, P.T. Guenther, J.W. Meadows, R.D. Lawson, R.J. Howerton, and T. Djemil, *Neutronic Evaluated Nuclear–Data File for Vanadium*, May 1988.

ANL/NDM–106 A.B. Smith, P.T. Guenther, and R.D. Lawson, *Fast–Neutron Elastic Scattering from Elemental Vanadium*, March 1988.

ANL/NDM–107 P. Guenther, R. Lawson, J. Meadows, M. Sugimoto, A. Smith, D. Smith, and R. Howerton, *An Evaluated Neutronic Data File for Elemental Cobalt*, August 1988.

ANL/NDM–108 M. Sugimoto, P.T. Guenther, J.E. Lynn, A.B. Smith, and J.F. Whalen, *Some Comments on the Interaction of Fast–Neutrons with Beryllium*, November 1988.

ANL/NDM–109 P.T. Guenther, R.D. Lawson, J.W. Meadows, A.B. Smith, D.L. Smith, and M. Sugimoto, *An Evaluated Neutronic Data File for Bismuth*, November 1989.

ANL/NDM–110 D.L. Smith and L.P. Geraldo, *A Vector Model for Error Propatation*, March 1989.

ANL/NDM–111 J.E. Lynn, *Fifty Years of Nuclear Fission*, June 1989.

ANL/NDM–112 S. Chiba, P.T. Guenther, and A.B. Smith, *Some Remarks on the Neutron Elastic– and Inelastic–Scattering Cross Sections of Palladium*, May 1989.

ANL/NDM–113 J.E. Lynn, *Resonance Effects in Neutron Scattering Lengths*, June 1989.

AMBIGUITIES IN THE ELASTIC SCATTERING OF 8 MeV NEUTRONS FROM ADJACENT NUCLEI

A. B. Smith, R. D. Lawson, and P. T. Guenther

ABSTRACT

Ratios of the cross sections for elastic scattering of 8 MeV neutrons from adjacent nuclei are measured over the angular range $\approx 20^0$–160^0 for the target pairs ^{51}V/Cr, ^{59}Co/^{58}Ni, Cu/Zn, ^{89}Y/^{93}Nb, ^{89}Y/Zr, ^{93}Nb/Zr, In/Cd and ^{209}Bi/Pb. The observed ratios vary from unity by as much as a factor of ≈ 2 at some angles for the lighter target pairs. Approximately half the measured ratios (Cu/Zn, In/Cd and ^{209}Bi/Pb) are reasonably explained by a simple spherical optical model, including size and isospin contributions. In all cases (with the possible exception of the ^{51}V – Cr pair), the geometry of the real optical–model potential is essentially the same for neighboring nuclei, and the real–potential strengths are consistent with the Lane model. In contrast, it is found that the imaginary potential may be quite different for adjacent nuclei, and the nature of this difference is examined. It is shown that the spin–spin interaction has a negligible effect on the calculation of the elastic–scattering ratios, but that channel coupling, leading to a large reorientation of the target ground state, can be a consideration, particularly in the ^{59}Co/^{58}Ni case. In the $A \approx 50$–60 region the calculated ratios are sensitive to spin–orbit effects, but the exact nature of this interaction must await more definitive polarization measurements. The measured and calculated results suggest that the concept of a conventional "global" or even "regional" optical potential provides no more than a qualitative representation of the physical reality for a number of cases.

I. INTRODUCTION

The elastic scattering of fast neutrons from spherical nuclei is conventionally described in terms of a spherical–optical–model potential (SOM), having real, imaginary, and spin–orbit components.[1] A number of "global"[2-5] and some "regional"[6] SOMs have been proposed, and it is interesting to investigate the validity of such global and regional concepts. A convenient way of exploring regional SOMs is to measure the ratios of elastic—neutron scattering from neighboring nuclei as a function of angle. This procedure has some distinct experimental advantages. If the measurements are made back–to–back, time dependent drifts of the experimental apparatus are very much mitigated. Uncertainties associated with comparisons of independent absolute measurements are largely avoided, as the difficult problem of calibrating the sensitivity of the apparatus and the absolute normalization of the resulting cross sections is no longer a factor in the interpretations. In addition, if the nuclear densities of the neighboring nuclei are similar, experimental uncertainties due to multiple–event, neutron–attenuation and angular–resolution effects tend to cancel out.

In order to examine the appropriateness of regional SOMs, we have carried out neutron elastic–scattering ratio measurements over a broad mass–range of target nuclei–specifically, the ratios ^{51}V/Cr, ^{59}Co/^{58}Ni, Cu/Zn, ^{89}Y/Zr, ^{89}Y/^{93}Nb, ^{93}Nb/Zr, In/Cd, and ^{209}Bi/Pb (the mass number is not given for those targets consisting of multi–isotopic components). Measurements were made at forty or more scattering angles distributed between $\approx 20^0$ and 160^0 at an incident–neutron energy of 8 MeV. The latter energy was chosen as it was experimentally favorable and, at the same time, is a low enough energy to be sensitive to nuclear-structure effects, yet high enough so that compound–elastic scattering (CE) is negligible. Thus, the observed elastic scattering should be essentially due to "shape elastic" (SE) processes. Section II of this paper gives a brief outline of the experimental methods employed in the above ratio measurements.

During the past few years there have been extensive measurements of neutron scattering from ^{51}V, ^{59}Co, ^{89}Y, ^{93}Nb, In, and ^{209}Bi over the 1.5–10 MeV range at this laboratory (as described in Refs. 7–12, respectively), and these results have been interpreted in terms of the SOM. Thus, with the exception of the Cu – Zn pair (and the TUNL group has proposed a SOM in this region[6]), a reliable SOM, which describes at least one member of the above–cited ratios, is known. Therefore, the question addressed in Sec. III is how well the measured ratio data can be explained by the respective regional SOMs, with variations in the potentials for the neighboring nuclei governed only by the common size effect (i.e., $R_i = r_i \cdot A^{1/3}$), and the isovector potential term of Lane.[13]

In Sec. IV, other effects that could contribute to the interpretation of the measured elastic–scattering ratios are discussed. These include: i) contributions from experimentally unresolved inelastic–neutron and CE scattering, ii) contributions from the spin–spin interaction, iii) collective deformation effects, iv) changes in both strengths and geometries of the SOM for neighboring nuclei, and v) variations in the spin–orbit interaction between neighboring nuclei. Finally, Sec. V includes some additional discussion and summary remarks.

II. EXPERIMENTAL METHOD

The measurements employed the time–of–flight technique, using the Argonne 10–angle detector system,[14] to resolve elastically–scattered neutrons, as far as possible, from those emitted non–elastically. The measurements were made at forty scattering angles distributed between 20^0 and 160^0. For most of the measurements, two angles (20^0 and 30^0) were redundantly used to test the reproducibility of the detection system. Generally, the measurements were made "back–to–back" in order to mitigate any possible time–dependent drifting of the apparatus. This ratio approach avoids a number of experimental difficulties, particularly the need to calibrate the sensitivity of the apparatus. The $D(d,n)^3He$ reaction was used as a neutron source throughout the measurements. The mean incident–neutron energy was (8.00 ± 0.01) MeV, and the incident–neutron energy spread ≈ 150 keV. The scattered–neutron resolution was ≈ 300 keV. All of the scattering samples were solid metal cylinders, 2 cm in diameter and 2 cm long, with neutrons incident on their lateral surface. The experimental results were corrected for multiple–event and neutron-attenuation effects using Monte–Carlo procedures.[15] In some of the ratios the nuclear densities of the respective samples were very similar (e.g., ^{59}Co and ^{58}Ni) and, assuming similar elastic–scattering and total cross sections, these corrections become negligible. However, in others (e.g., ^{93}Nb and Zr) the densities were quite different, and the corrections are significant, 5% or more in the ratio values at some angles. Care was taken to assure that the correction procedures were accurate. As scattered–neutron intensities varied with angle by more than two orders of magnitude in some cases, statistical uncertainties changed from $< 1\%$ to $\geq 10\%$ (including foreground, background, and multiple–event–correction contributions) depending upon scattering angle. The statistical uncertainties were propagated through the experimental data analysis. Details of the experimental methods are given in Refs 14 and 16–18.

III. EXPERIMENTAL RESULTS, SIZE AND ISOSPIN PREDICTIONS

The measured $^{51}V/Cr$, $^{59}Co/^{58}Ni$, Cu/Zn, $^{89}Y/Zr$, $^{89}Y/^{93}Nb$, $^{93}Nb/Zr$, In/Cd, and $^{209}Bi/Pb$ elastic–scattering ratios at an incident neutron energy of 8 MeV are shown in Figs. 1 to 8. Although the measurements were made "back–to–back" in order to obtain, insofar as possible, identical experimental conditions, there remain possible systematic experimental uncertainties; e.g., very small short–term shifts in the position of the neutron source can lead to significant systematic variations in the measured ratios at forward angles where the cross sections are changing very rapidly with angle. No subjective attempt was made to quantify the latter and other systematic uncertainties, and in the figures only statistical uncertainties are shown.

At 8 MeV, SOM interpretations of neutron elastic scattering are usually based on a real Woods–Saxon potential, together with an imaginary derivative–Woods–Saxon well and a Thomas spin–orbit potential.[1] Unless otherwise stated, these spherical potential forms are assumed in the present interpretation. The radii are taken to have the form $R_i = r_i \cdot A^{1/3}$, where the reduced radii ($r_i = r_v$, r_w and r_{so} for the real, imaginary and spin–orbit potentials, respectively), together with the respective potential diffusenesses (a_v, a_w and a_{so}), are assumed identical for neighboring nuclei. The isovector Lane potential,[13]

$$U = -4\, U_1\, \vec{t}\cdot\vec{T}/A, \tag{1}$$

where $\vec{t}$ and $\vec{T}$ are the isospin operators for the projectile and target respectively, can affect the prediction of cross–section ratios. For neutron scattering, without charge exchange, only the $t_z T_z$ component of $\vec{t}\cdot\vec{T}$ is important, and the consequence of Eq. 1 is the addition of a term to the usual real and imaginary SOM potentials so that they become

$$V = V_0(r) - V_1(r)\,(N - Z)/A \tag{2}$$

and

$$W = W_0(r) - W_1(r)\,(N - Z)/A, \tag{3}$$

where $(N - Z)/A$ is the neutron excess in the target divided by the total number of target nucleons, A. Throughout these remarks, it is assumed that the geometries of the isovector potentials, $V_1(r)$ and $W_1(r)$, are the same as those of $V_0(r)$ and $W_0(r)$, respectively. The strengths of the isovector contributions at 8 MeV were taken from the work of Walter and Guss,[5]

$$V_1 = 15.85 \text{ MeV}$$

and (4)

$$W_1 = 14.94 \text{ MeV}.$$

Some of the measurements employed multi–isotopic elemental targets. In these cases, the calculations were carried out on an isotopic basis, and the results were combined, weighted by the natural abundance of the respective isotopes,[19] to obtain the elemental values. Throughout this section, only the size and isovector effects are considered, and the strengths of the spin–orbit potentials are assumed identical for a given pair.

A. The ^{51}V/Cr Ratio

Vanadium (99.75% ^{51}V) and chromium (83.79% ^{52}Cr) are approximately spherical nuclei.[20] The even chromium isotopes (90.5% elemental abundance) have first–excited states that are at sufficiently high excitation energies to allow clear resolution of elastically and inelastically scattered neutrons in the present measurements. On the other hand, ^{51}V ($7/2^-$) has a low–lying excited ($5/2^-$) level at 320 keV,[21] and any inelastically scattered neutrons resulting from the excitation of this state were not resolved from the elastically scattered contribution in the present measurements. Such inelastic contributions due to compound–nucleus (CN) processes are negligibly small, but a direct–reaction component may be appreciable, as outlined in Sec. IV. The measured ratios of the ^{51}V/Cr elastic scattering are shown in Fig. 1, and, for reference, the lower portion of the figure indicates the corresponding ^{51}V elastic–scattering angular distribution. The measured ratios differ substantially from unity over most of the angular range, approaching 2 at $\approx 150^\circ$. The ratio maxima occur near, but not exactly at, the minima of the ^{51}V (and Cr) elastic–scattering distribution(s).

Theoretically predicted ratios are also shown in Fig. 1. These are based upon the vanadium SOM of Ref. 7 (given at 8 MeV in Table 1), which was obtained from an analysis

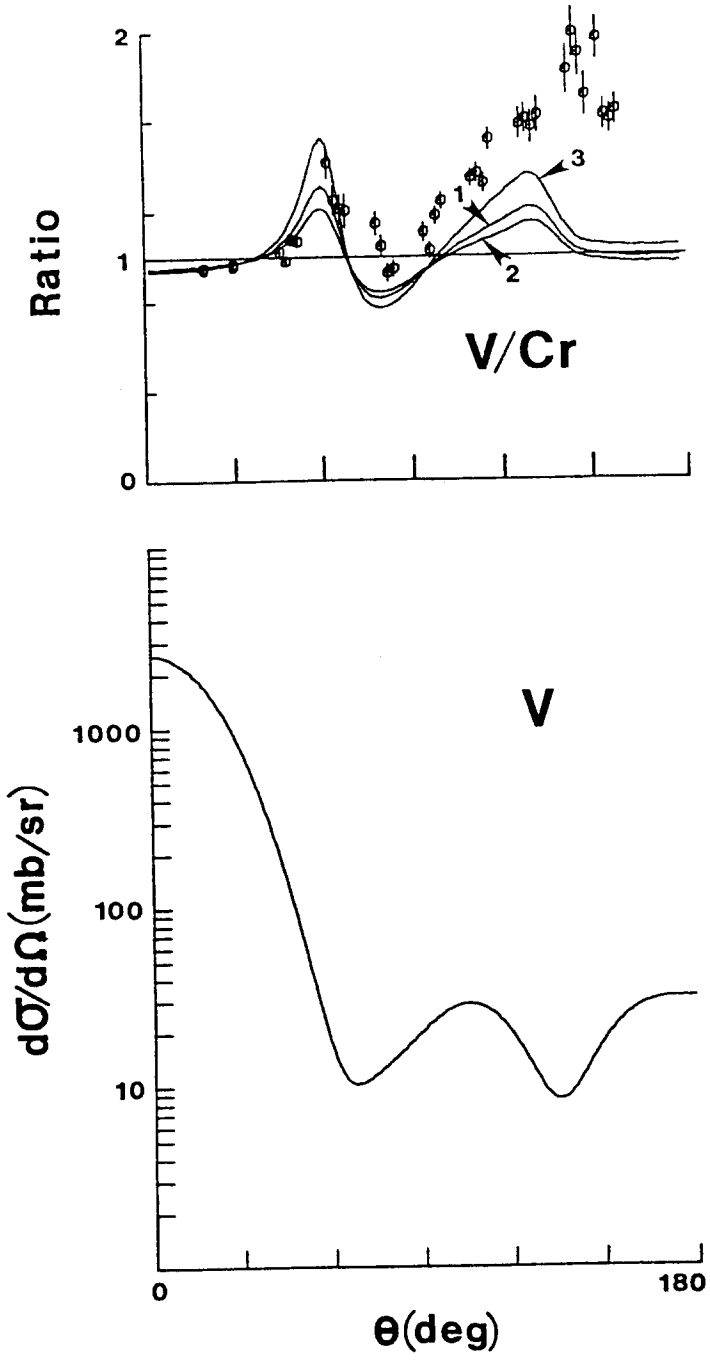

Fig. 1. The $^{51}V/Cr$ elastic–scattering ratio at an incident–neutron energy of 8 MeV (upper portion of the figure). The measured values are indicated by "O" symbols and the results of calculations by curves. The curves correspond to isovector potentials of Eq. 4 (1), half that strength (2), and twice that strength (3), as described in the text. The lower portion of the figure shows the corresponding ^{51}V differential elastic–scattering cross sections as calculated with the potential of Ref. 7. All the data are given in the laboratory coordinate system.

Table 1

Spherical optical–model potentials used, in conjunction with Eqs. 2 to 4 of the text, to calculate the elastic–scattering cross–section ratios. The parameter values were obtained from interpretations of experimental data as described in the references cited in the text. The real potential has the Woods–Saxon shape, the imaginary potential a derivative Woods–Saxon shape, and the spin–orbit potential the Thomas form. The potential strengths (V_o, W_o and V_{so}) are in MeV, and the radii (r_i) and diffusenesses (a_i) in fms.

	Real Potential		
Nucleus	V_{oo}	r_v	a_v
^{51}V	44.125	1.2680	0.6147
^{58}Ni	47.724	1.2538	0.6461
^{59}Co	46.324	1.2624	0.6355
^{89}Y	45.852	1.2400	0.7033
^{93}Nb	45.280	1.2500	0.7000
In	44.596	1.2500	0.6901
^{209}Bi	46.401	1.2200	0.7000
	Imaginary Potential		
	W_{oo}	r_w	a_w
^{51}V	6.016	1.2997	0.4839
^{58}Ni	10.747	1.1902	0.5093
^{59}Co	9.094	1.2119	0.4800
^{89}Y	8.371	1.3296	0.3933
^{93}Nb	8.435	1.3000	0.4700
In	7.835	1.3011	0.4585
^{209}Bi	5.958	1.3102	0.4900
	Spin–Orbit Potential		
	V_{so}	r_{so}	a_{so}
^{51}V	8.360	1.000	0.6500
^{58}Ni	5.500	1.005	0.6500
^{59}Co	5.500	1.005	0.6500
^{89}Y	5.750	1.025	0.4000
^{93}Nb	6.000	1.250	0.7000
In	5.500	1.000	0.6500
^{209}Bi	5.220	1.005	0.6500

of 1.5–10 MeV elastic–scattering data. The calculated ratios considered only the $A^{1/3}$ size effect on the SOM radii, and the $(N - Z)/A$ isovector terms of Eqs. 2, 3, and 4. Three calculated–ratio curves are shown in Fig. 1. The "1" curve was obtained using the isovector strengths of Walter and Guss, Eq. 4. The other two curves were obtained by: i) halving the Walter and Guss isovector strengths ("2" curve), and ii) doubling them ("3" curve). From these comparisons of measured and calculated ratios, it is clear that size and isovector changes in the SOM potential alone do not explain the observed $^{51}V/Cr$ elastic–scattering ratios, particularly at the larger scattering angles.

B. The $^{59}Co/^{58}Ni$ Ratio.

Cobalt (100% ^{59}Co, $7/2^-$) and ^{58}Ni (fully–enriched sample, 0^+) have relatively high–energy first–excited states,[22-23] making possible the experimental resolution of the elastically–scattered neutrons at all angles in the present work. The character of the elastic–scattering ratios, shown in Fig. 2, is similar to that of the $^{51}V/Cr$ ratio, except that the first maximum at $\approx 60^o$ is not as pronounced, the ratios do not approach unity in the 80^o–90^o region, and the broad large maximum of the ratio is at $\approx 120^o$ rather than $\approx 150^o$. The lower portion of Fig. 2 shows the corresponding ^{59}Co elastic–scattering distribution calculated from the potential of Ref. 8. It is evident that the maxima of the measured ratios occur near the minima of the elastic distribution.

The $^{59}Co/^{58}Ni$ theoretical ratio predictions were based upon the SOM of Ref. 8 (given in Table 1). That model was deduced from an extensive set of elastic–scattering measurements extending over the 1.5–10 Mev energy range. In calculating the ratios, the $A^{1/3}$ size effect and the isovector contributions defined by Eqs. 2, 3, and 4 were taken into consideration. It is evident that the calculated ratios (curve "1" of Fig. 2) are much smaller than those observed, particularly in the neighborhood of 60^o and 120^o. Doubling the isovector strengths (curve "3") leads to calculated results approaching the large maximum at $\approx 120^o$, but worsens the agreement with experiment in the 60^o–80^o range. Halving the isovector strengths (curve "2") leads to calculated results much smaller than the measured values over the large majority of the angular range. Thus, as in the $^{51}V/Cr$ case, the SOM, with simple size and isovector contributions, does not explain the observed $^{59}Co/^{58}Ni$ elastic–scattering ratios.

C. The Cu/Zn Ratio

The experimental Cu/Zn elastic–scattering ratios, shown in Fig. 3, were obtained using elemental copper (69.17% ^{63}Cu and 30.83% ^{65}Cu, both with $J^\pi = 3/2^-$), and elemental zinc (consisting 95.9% of $^{64,66,68,70}Zn$). The first–excited states of the even isotopes of zinc are at energies of $>\approx 0.9$ MeV;[24] thus inelastic–neutron contamination of the measured elastic–scattering ratios was limited to the 4.1% abundant ^{67}Zn and was ignored. The first–excited states of the two copper isotopes are at lower energies, ≈ 0.7 MeV, and the corresponding inelastically–scattered neutrons were only marginally resolved in the present measurements at large scattering angles. The measured elastic–scattering ratios, Fig. 3, exhibit at least two maxima, at approximately 50^o and 110^o, and these are near the minima of the copper elastic–scattering distributions shown in the lower portion of the figure. The peaks in the ratio are much weaker than in the $^{51}V/Cr$ and $^{59}Co/^{58}Ni$ cases. The root–mean–square (RMS) deviation of the Cu/Zn ratios from unity is 0.133,

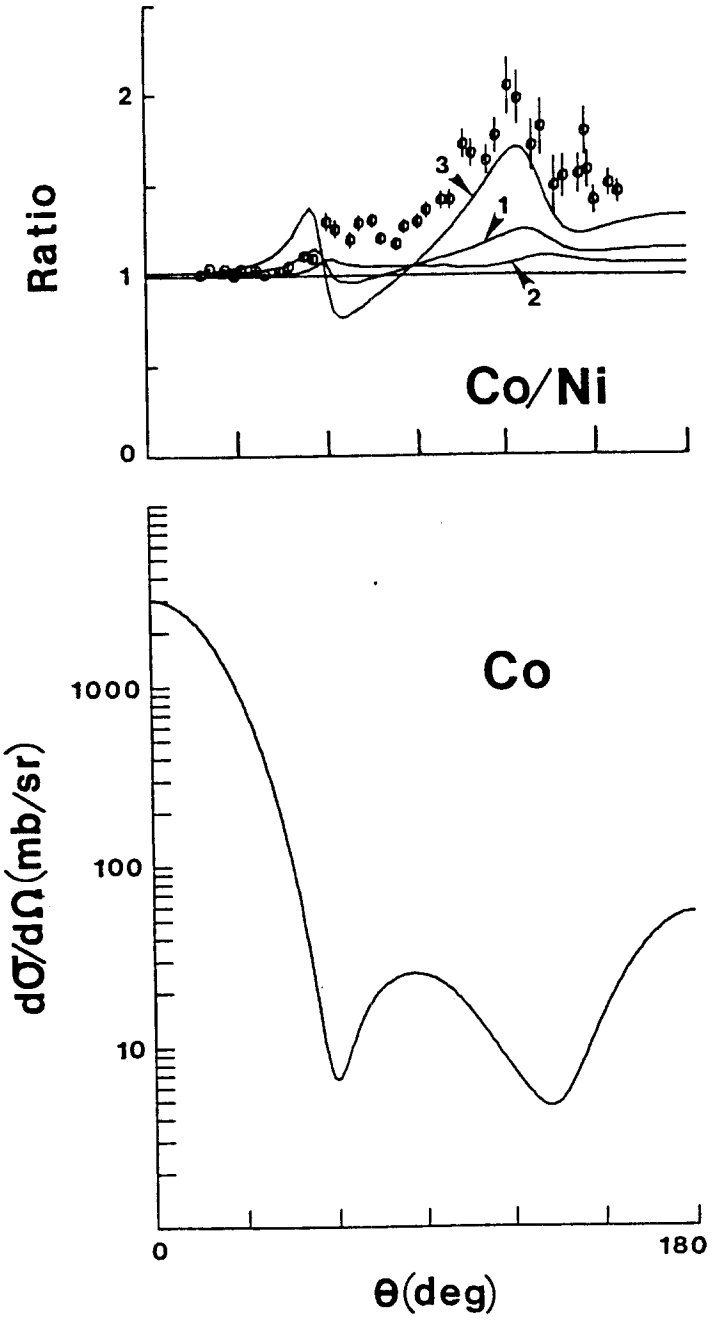

Fig. 2. Comparison of measured and calculated $^{59}Co/^{58}Ni$ elastic–scattering ratios at an incident neutron energy of 8 MeV (upper portion of the figure). The notation is the same as for Fig. 1, except that the calculations are based upon the potential of Ref. 8, as described in the text. The lower portion of the figure shows the corresponding ^{59}Co differential elastic–scattering cross section. The data are given in the laboratory coordinate system.

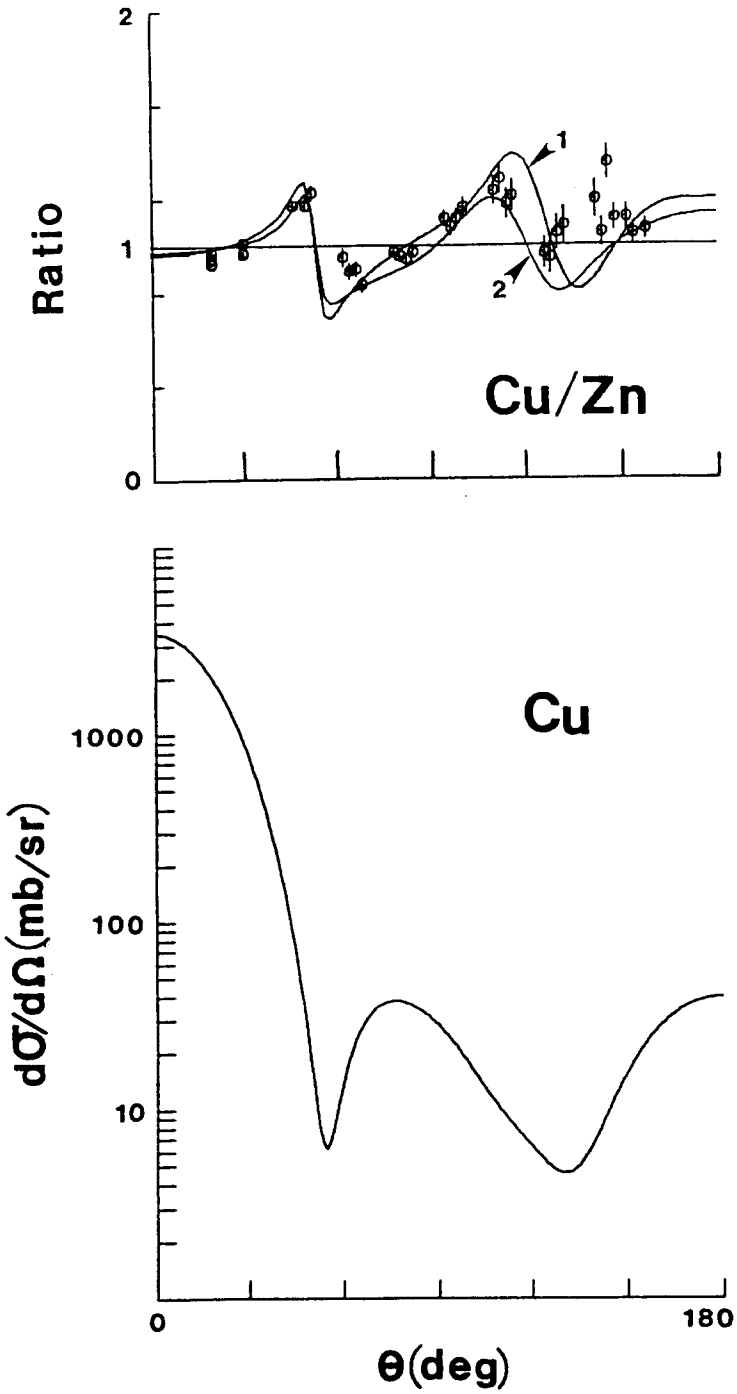

Fig. 3. Comparison of measured and calculated Cu/Zn elastic–scattering ratios at an incident neutron energy of 8 MeV (upper portion of the figure). The "1" and "2" curves correspond to alternate choices of the Cu SOM as described in the text. The corresponding Cu differential elastic–scattering cross section is shown in the lower portion of the figure. The data are given in the laboratory coordinate system.

compared to the analogous values of 0.434 and 0.467 for the $^{51}V/Cr$ and $^{59}Co/^{58}Ni$ ratios, respectively.

The average $(N - Z)/A$ of elemental copper and zinc are similar, thus the isovector term of the potential will have very little effect on the calculation of the elastic–scattering ratios. The elastic–scattering from zinc was calculated using the "Fe and Cu model" given in Table 5 of the paper of El–Kadi et al.[6] The copper cross sections were calculated in two ways: first using the regional model of the zinc calculations, and, second, using the ^{63}Cu and ^{65}Cu SOM parameters of Table 2 of the El–Kadi et al. paper. Figure 3 shows the results obtained using these two alternate methods, curves "1" and "2", respectively. There is a modest difference between the two calculated results, and both give elastic–scattering ratios in reasonable agreement with experiment. The discrepancies between measured and calculated ratios are largest in the 130°–150° angular region where there may be a distortion of the experimental values due to the incomplete resolution of the first inelastically–scattered neutron group from the copper isotopes. Thus, the regional SOM of El–Kadi et al., together with the $A^{1/3}$ size effect, reasonably describes the measured Cu/Zn elastic–scattering ratios.

D. The $^{89}Y/Zr/^{93}Nb$ Ratios

Near A = 90 three elastic–scattering ratios were measured: $^{89}Y/Zr$, $^{93}Nb/Zr$ and $^{93}Nb/^{89}Y$. Yttrium (100% ^{89}Y, $1/2^-$) and niobium (100% ^{93}Nb, $9/2^+$) are near the N = 50 shell closure and essentially spherical. The first excited state of ^{89}Y is at a relatively high energy (≈ 0.9 MeV),[24] and inelastic–neutron excitation of this state involves both a parity change and a large spin change, $\Delta I = 4$. Consequently, the corresponding inelastic–scattering cross section is small at 8 MeV, and inelastic–scattering perturbations of the observed elastic scattering from ^{89}Y are not a concern in the present measurements. There is a low–lying isomeric state in ^{93}Nb (at ≈ 30 keV, $1/2^-$),[24] but again there is a large spin change, $\Delta I = 4$, and a change of parity in the corresponding inelastic–scattering processes. The respective inelastic–scattering cross section is known to be very small at much lower energies, and thus was ignored in the present considerations. The next levels in ^{93}Nb are a quartet of states, with excitation energies ranging from 687 to 810 keV. For these, the experimental resolution of the scattered–neutron components was similar to that outlined above for copper. More than half of elemental zirconium is ^{90}Zr, which has a first–excited state at 1.76 MeV. Thus, for this isotope, the measured elastic–neutron scattering was completely resolved. The remaining isotopes of the element have first–excited states[24] with energies of >≈ 918 keV, so inelastic–neutron distortions of the observed elastic scattering from elemental zirconium were essentially negligible.

The measured $^{89}Y/Zr$ elastic–scattering ratios are shown in Fig. 4. They differ from the Cu/Zn results in that the magnitudes of the maxima at ≈ 95° and 150° are somewhat greater, and there is a systematic trend for the ratios to become larger than unity as the angle increases. Furthermore, the ^{89}Y elastic–scattering cross sections, shown in the lower portion of Fig. 4, exhibit three minima, in contrast to the two of the lighter targets. In the vicinity of the first minimum, ≈ 50°, the measured ratios are near unity, a distinct difference from the results shown in Figs. 1 and 2 where the minima of the elastic–scattering cross sections tend to correspond to a maximum of the cross–section ratios.

The measured $^{93}Nb/Zr$ elastic–scattering ratios are shown in Fig. 5. Although they appear markedly different from the results of Fig. 4, the RMS deviation from unity is quite

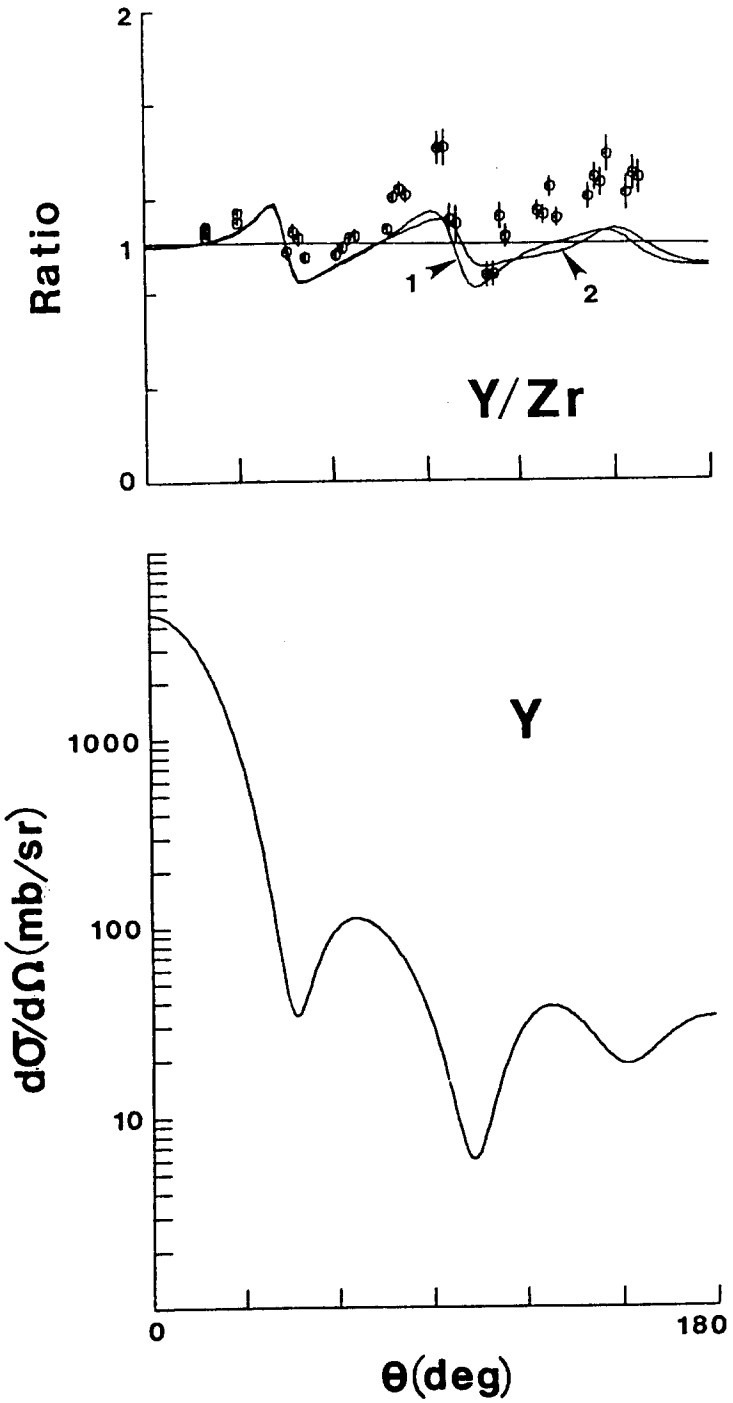

Fig. 4. Comparison of measured and calculated $^{89}Y/Zr$ elastic–scattering ratios at an incident neutron energy of 8 MeV (upper portion of the figure). The experimental values are indicated by "O" symbols, and the results of calculations by curves, as described in the text. The associated ^{89}Y differential elastic–scattering cross section is given in the lower portion of the figure. The data are given in the laboratory coordinate system.

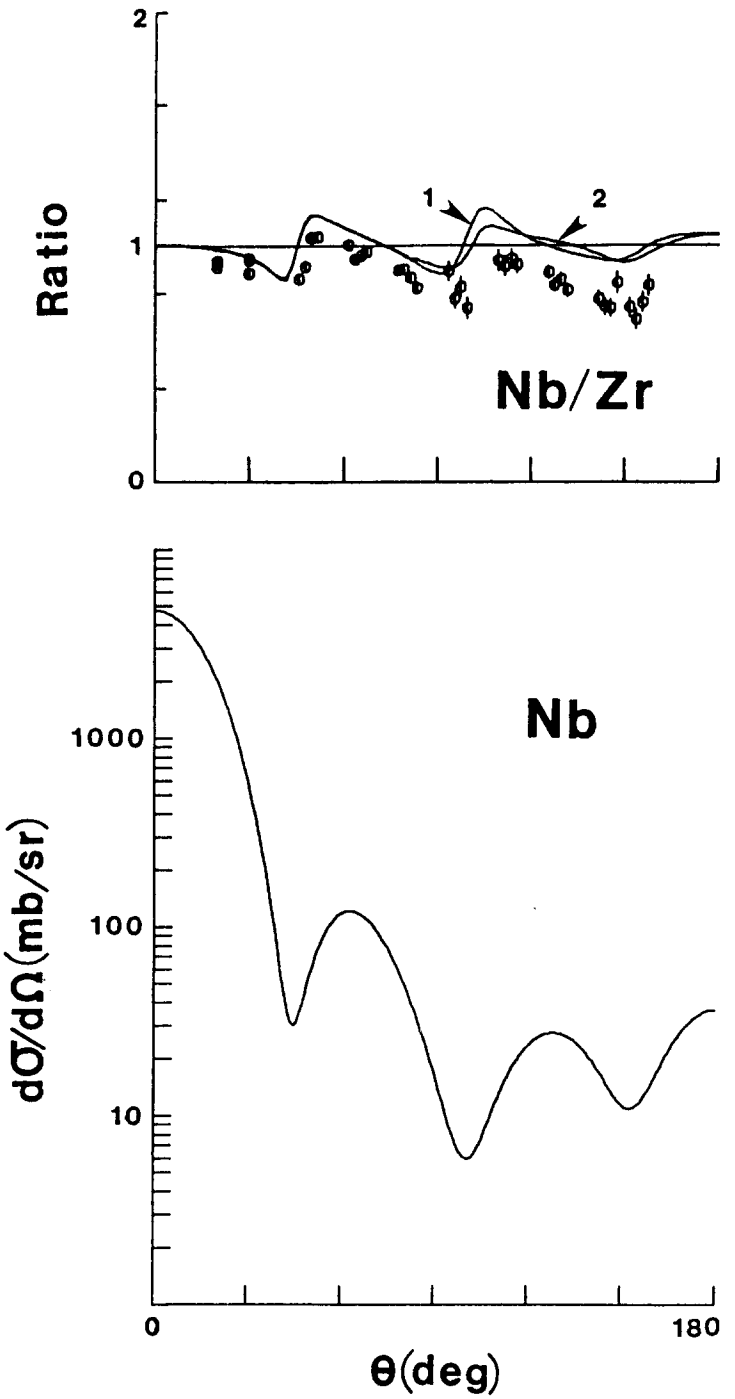

Fig. 5. Comparison of measured and calculated ^{93}Nb/Zr elastic–scattering ratios at an incident neutron energy of 8 MeV (upper portion of the figure). The experimental values are indicated by "O" symbols, and the results of calculations by curves, as described in the text. The associated ^{93}Nb differential elastic–scattering cross section is given in the lower portion of the figure. The data are given in the laboratory coordinate system.

similar (0.150 and 0.180 for ^{93}Nb/Zr and ^{89}Y/Zr ratios, respectively), and Fig. 5 is very similar to an inverse of Fig. 4. The respective ^{93}Nb elastic–scattering cross sections are shown in the lower portion of Fig. 5, and the same comments made above, relevant to ^{89}Y, apply.

Finally, the independently measured ^{93}Nb/^{89}Y elastic–scattering ratios, shown in Fig. 6, follow the trend of the ^{93}Nb/Zr ratios, but the deviation from unity is much more pronounced, as it must be if the three sets of experiments are to be consistent. This is reflected in the RMS deviation from unity of the measured ^{93}Nb/^{89}Y ratios of 0.254, approximately twice as large as that of the other two pairs of the triad.

Theoretical estimates of the elastic–scattering cross–section ratios in the $A \approx 90$ region were made in two different ways. In the first approach, the SOM of ^{89}Y, deduced from 1.5–10 MeV elastic–scattering measurements at this laboratory[9] (see parameters given in Table 1), was used as the basic model. The results of the calculations using this approach are indicated by the "1" curves in Figs. 4 to 6, where the $A^{1/3}$ size effect and the isovector potentials of Eqs. 2 to 4 were taken into account. The $(N - Z)/A$ values in this mass region are very similar; thus, the isovector effect is small. The second, and similar, approach used as the basic SOM the ^{93}Nb potential given in Ref. 10, and Table 1. That potential also was derived at this laboratory from an extensive study of the elastic scattering of 1.5–10 MeV neutrons from niobium. Again, taking account of the $A^{1/3}$ size effect and the isovector potentials, the calculated ratios indicated by the "2" curves of Figs. 4 to 6 were obtained. The results obtained with the two different SOM bases are quite similar. Near 90° the predicted ^{93}Nb/Zr ratios are in reasonable agreement with the observed values, but there are some differences between measured and calculated results for the ^{89}Y/Zr and ^{93}Nb/^{89}Y ratios. In the 130° –150° range, all three calculated ratios are considerably different from the measured values. Thus, the simple $A^{1/3}$ size effect, together with the minor contribution from the isovector potentials, does not explain the experimental elastic–scattering ratios in the $A \approx 90$ region.

On the other hand, the ^{93}Nb/^{89}Y elastic–scattering ratios calculated with the independently derived SOM of Refs. 9 and 10 are in good agreement with the observed ratio values, as illustrated by the "3" curve of Fig. 6. This illustrates the consistency of the three independent data sets (^{93}Nb scattering, ^{89}Y scattering, and ^{93}Nb/^{89}Y ratios), obtained over a span of about five years. The modest discrepancies near $\approx 50°$ are probably due to multiple–event effects which were not as rigorously treated in the early ^{93}Nb measurements as in the later ^{89}Y measurements.

E. The In/Cd Ratio

Elemental indium consists of ^{115}In (95.7%) and ^{113}In, both with $9/2^+$ ground states and a low–lying metastable $1/2^-$ first–excited level (at 336 and 392 keV, respectively).[24] Inelastically–scattered neutrons due to the excitation of these first–excited levels were not resolved from the elastically–scattered component in the present measurements. However, the large spin change, $\Delta I = 4$, and parity change imply very small CN and/or direct inelastic–scattering cross sections for these two levels, and observation supports this assumption at lower incident energies.[17] The next excited state in ^{115}In is at 597.1 keV $(3/2^-)$,[25] and the corresponding inelastically–scattered neutrons were only partially resolved from the elastically–scattered component. This state, together with the 1.0415 MeV $(5/2^-)$ level,[16] has a center–of–gravity[26] which is 528 keV above the first–excited $1/2^-$

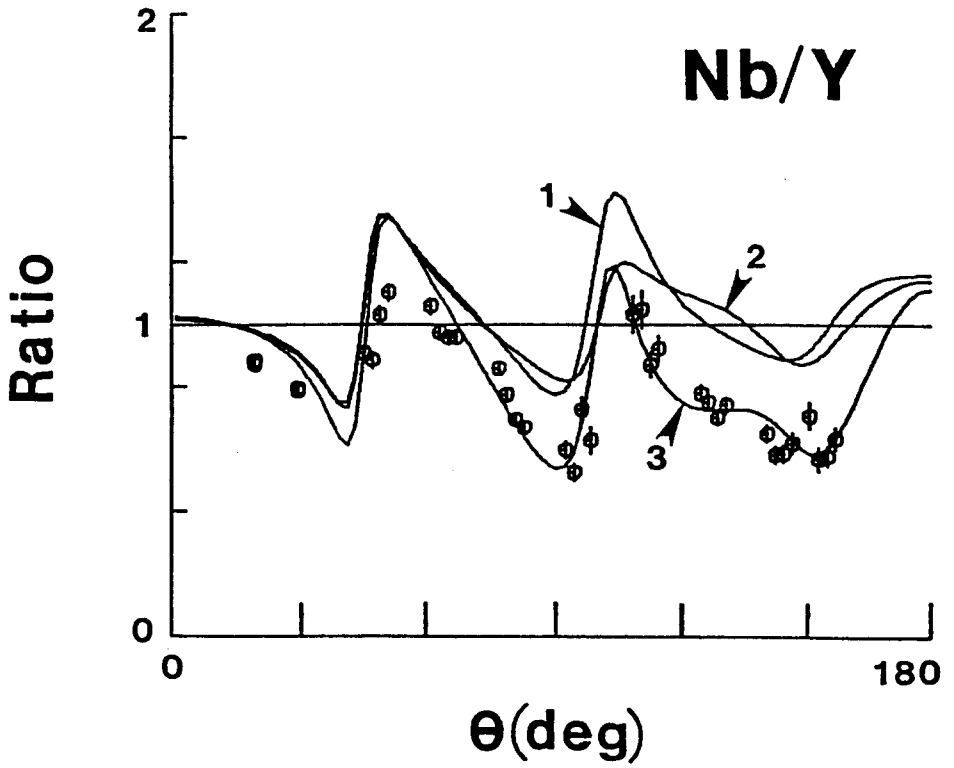

Fig. 6. Comparison of measured and calculated $^{93}Nb/^{89}Y$ elastic–scattering ratios at an incident neutron energy of 8 MeV. The experimental values are indicated by "O" symbols, and the results of calculations by the curves, as described in the text. The data are given in the laboratory coordinate system.

level, in good agreement with the 2^+ excitation energy[24] in ^{114}Cd, 558 keV. Thus a reasonable interpretation of this $3/2^-$ level is a $p_{1/2}$ proton coupled to the yrast 2^+ state of the ^{114}Cd core. Since the ground state of ^{115}In is a $g_{9/2}$ proton coupled to the 0^+ ^{114}Cd core, inelastic scattering due to the excitation of the $3/2^-$ level should be small (and not a concern in the ratio measurements), and this is born out by lower–energy neutron–scattering measurements.[17] The same arguments hold true for ^{113}In but the isotope is of such small natural abundance that it can be ignored in the present considerations.

Approximately 75% of elemental cadmium consists of even isotopes, having 2^+ first–excited states ranging in energy from 500 to 650 keV.[19,24] The remaining $\approx$ 25% of the element is about equally divided between ^{111}Cd and ^{113}Cd, and both isotopes have several excited states below 600 keV. The present measurements suggest that the inelastic–scattering component due to the direct excitation of low–lying levels in the even isotopes of cadmium is significant at an incident energy of 8 MeV, and it is only partially resolved from the elastically–scattered contribution. Thus, there is considerable uncertainty in the observed "elastic" scattering from cadmium in the present measurements at large scattering angles, and there may be significant inelastic perturbations at other angles where the elastic–scattering cross section is at a minimum. With these caveats, the measured In/Cd elastic–scattering ratios are shown in Fig. 7. They fluctuate about unity by small amounts, except possibly at angles $\geq 135^o$ where the inelastic–scattering perturbations may be significant, as cited above.

The In/Cd elastic–scattering ratios were calculated using the In potential of Ref. 11, based upon extensive studies of 1.5–14.6 MeV elastic scattering from indium at this laboratory. The relevant indium elastic–scattering distribution is shown in the lower portion of Fig. 7. As before, size and isovector effects (with strengths given by Eq. 4) were taken into account, and the various isotopes were treated separately and then combined into a weighted elemental average. The latter is a significant point when dealing with the eight isotopes of cadmium. The calculated elastic–scattering ratios are in reasonable agreement with the measured values, as indicated by the curve in the upper portion of Fig. 7. Appreciable discrepancies occur only at large scattering angles, where the measured data are less reliable due to the resolution uncertainties noted above. Furthermore, better resolution in the cadmium measurements would lead to ratio values nearer unity, and in better agreement with the calculation. In view of these experimental uncertainties, it was concluded that the simple isovector and size dependencies of the SOM provide a reasonable explanation of the In/Cd elastic–scattering ratios.

F. The ^{209}Bi/Pb Ratio

Elemental bismuth (100% ^{209}Bi, $9/2^-$) and lead (77.9% even isotopes and more than 50% ^{208}Pb, 0^+) are essentially spherical nuclei. The experimental resolution was sufficient to separate elastically and inelastically scattered neutrons in the case of bismuth, where the first–excited state, at $\approx$ 900 keV, is not strongly excited.[27] The resolution of the elastically–scattered component from ^{208}Pb was complete, since the first–excited state (3^-) lies above 2 MeV, and, for the other even isotopes (^{204}Pb and ^{206}Pb), the resolution of the elastic–scattering component was similar to that of the bismuth case.[24] The first two excited states in ^{207}Pb lie at $\approx$ 570 ($5/2^-$) and 898 ($3/2^-$) keV. In these cases the experimental resolution of the elastic–scattering component was marginal, but the isotope is only 22.1% abundant. The measured ^{209}Bi/Pb elastic–scattering ratios are shown in Fig.

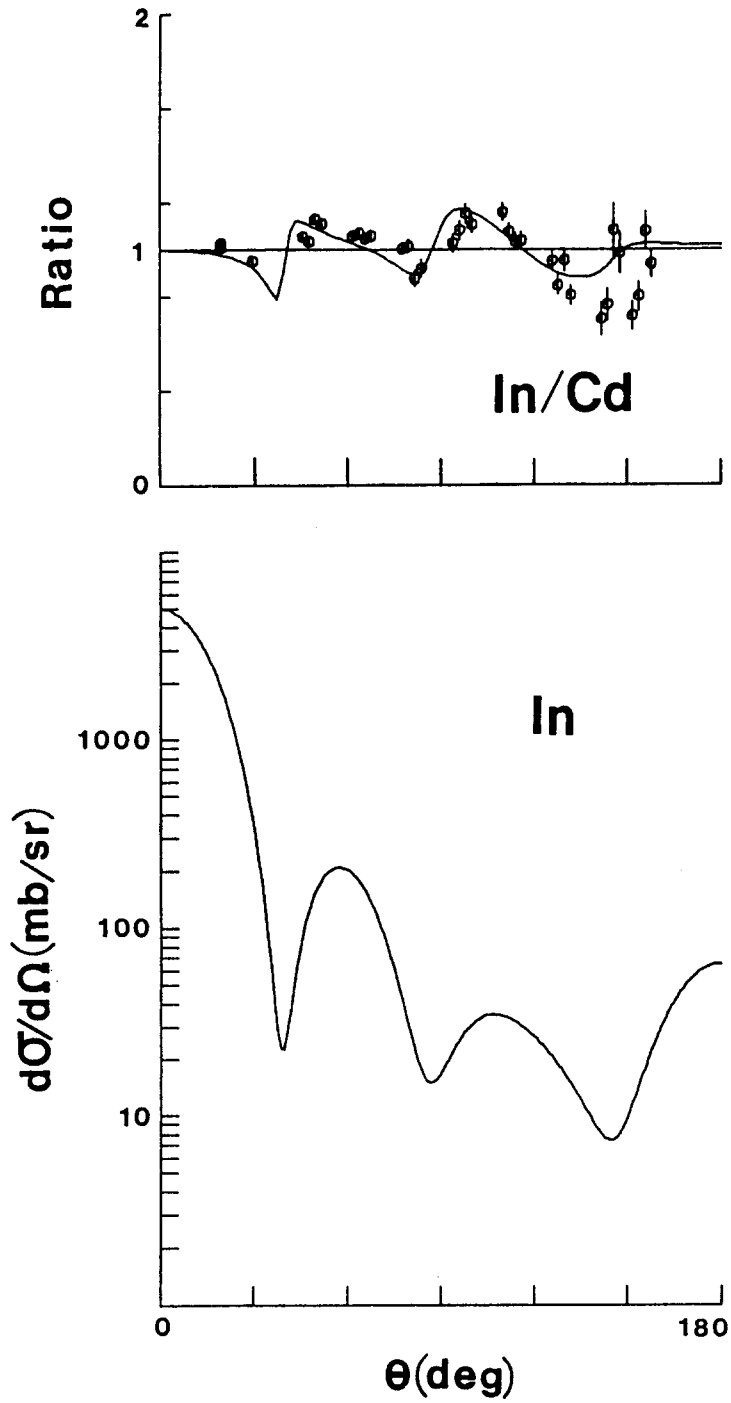

Fig. 7. Comparison of measured and calculated In/Cd elastic–scattering ratios at an incident neutron energy of 8 MeV (upper portion of the figure). Symbols indicate measured values and the curve the result of calculation, as described in the text. The lower portion of the figure shows the corresponding indium elastic–scattering distribution, as described in the text. The data are given in the laboratory coordinate system.

8. They are very near unity throughout the measured angular range, with fluctuations about unity that are only slightly beyond the experimental uncertainties.

The theoretical ^{209}Bi/Pb ratios, shown in the upper portion of Fig. 8, were calculated using the ^{209}Bi potential of Ref. 12 (and given in Table 1). The lower portion of this figure shows the corresponding ^{209}Bi elastic–scattering angular distribution. Because the $(N - Z)/A$ of these two targets, and the nuclear sizes, are very similar, neither the isovector potentials of Eqs. 2 to 4, nor the $A^{1/3}$ size effect are of appreciable consequence. Therefore, the calculated elastic–scattering ratios fluctuate about unity by only small amounts, and quite reasonably follow the experimental results. Thus, the observed ^{209}Bi/Pb elastic–scattering ratios are well described by the simple SOM, with a $A^{1/3}$ size dependence and the isovector strengths of Eq. 4.

IV. OTHER CONSIDERATIONS

From the foregoing analyses it is evident that, in about half the cases (i.e., for Cu/Zn, In/Cd and ^{209}Bi/Pb), the observed 8 MeV elastic–scattering ratios follow quite closely the predictions of the SOM, inclusive of $A^{1/3}$ size and isovector real– and imaginary–potential effects. On the other hand, the observed ^{51}V/Cr and ^{59}Co/^{58}Ni ratios, and the ratios near $A \approx 90$, are not consistent with the conventional SOM predictions. Underlying these conclusions is the assumption that at 8 MeV the elastic scattering is described by shape–elastic processes, with no significant compound–elastic (CE) contribution. Calculations indicate that the CE cross section is small in all presently studied cases ($\lesssim 3$ mb, or $<< 1$ mb/sr, which is below the sensitivity of the present measurements). Furthermore, at a given excitation energy, the density of states in an even–A target is smaller than in its odd–A neighbor, and thus one expects the CE contribution to be larger for the even–A member of the pair. At least in the ^{51}V/Cr and ^{59}Co/^{58}Ni cases, a contribution from the CE scattering would tend to make the ratios closer to unity, in contrast to the experimental observation. Therefore, the inclusion of CE scattering does not resolve the above discrepancies between measured and calculated ratios.

Near $A \approx 90$ it is known that the imaginary portion of the SOM is changing rapidly with target mass.[28] This is illustrated by the parameters of Table 1, which result in a J_w (the volume integral–per–nucleon of the imaginary potential) for ^{93}Nb that is 14.2% larger than that for ^{89}Y. This is an example of the fact that near shell closures, J_w is at a minimum and increases quite rapidly as one moves away from the magic number.[29-30] Physically, this is a manifestation of the fact that closed–shell nuclei have fewer low–lying excited states, and, as a consequence, fewer inelastic channels are open, and thus a smaller imaginary potential is needed to account for channels not otherwise explicitly addressed in the calculations. The closed–shell core in this instance is the $^{88}_{38}Sr_{50}$ nucleus, and, although $Z = 38$ is not a major shell closure, it has been established that the low–lying states of the $Z > 38$, $N = 50$ isotones can be well understood in terms of $p_{1/2}$ and $g_{9/2}$ protons moving outside this core.[31] Thus, it is not surprising that an SOM for Zr, based upon either that for ^{89}Y or ^{93}Nb, using Eqs. 2 to 4, does not fit the observed ratio data.

The other two pairs (^{51}V/Cr and ^{59}Co/^{58}Ni) for which the SOM has difficulty involve fairly light nuclei, and often for such light nuclei at few–MeV energies, the fundamental assumption of the SOM, namely, that the cross–section resonance structure is

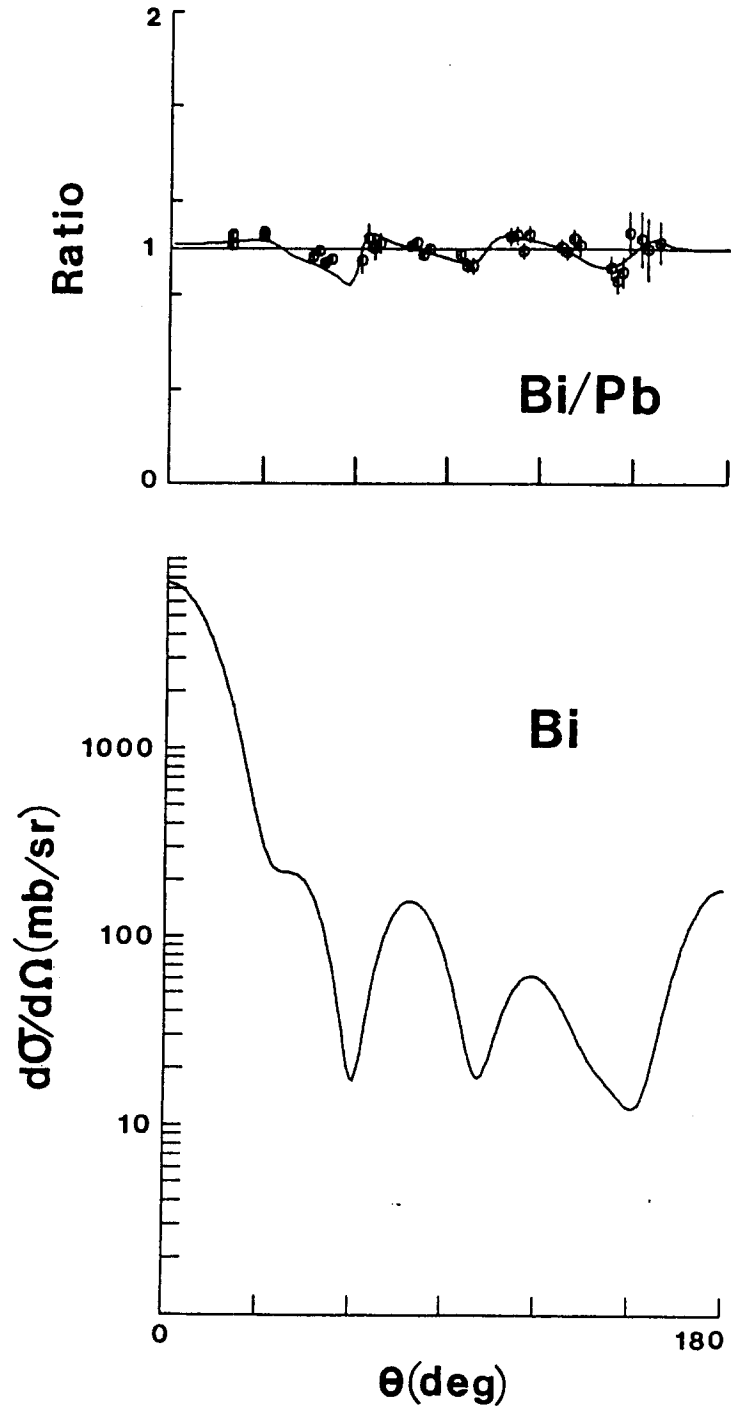

Fig. 8. Comparison of measured and calculated ^{209}Bi/Pb elastic scattering ratios at an incident neutron energy of 8 MeV (upper portion of the figure). Symbols indicated measured ratio values and curves calculated results as described in the text. The relevant differential elastic–scattering cross section of ^{209}Bi is shown in the lower portion of the figure. The data are given in the laboratory coordinate system.

fully overlapping resulting in energy–smooth cross sections, has only marginal validity. In addition, there are at least two other reasons why the simple SOM may have trouble explaining the observed values in these two cases. First, ^{51}V has a low–lying state at 320 keV ($5/2^-$), and inelastic–neutron–scattering due to the excitation of this level was not resolved from the elastically–scattered contribution in the present measurements. If some direct inelastic–scattering process were exciting this low–lying level, there could be a significant contribution to the observed "elastic" scattering, particularly near the minima of the vanadium differential elastic–scattering cross section, resulting in a distortion of the observed ^{51}V/Cr elastic–scattering ratios. Secondly, for spherical nuclei the radius of the real SOM is generally smaller than that of the imaginary potential.[28] As is evident in the numerical values of Table 1, the SOMs for ^{59}Co and ^{58}Ni violate this rule, and it has been shown that such a behavior of the SOM may indicate nuclear deformation.[8]

In the subsequent portions of this section, the above–cited and other effects possibly contributing to the anomalous elastic–scattering ratios are examined.

A. The Imaginary Potential Near A ≈ 90

For both ^{89}Y and ^{93}Nb, $(N - Z) = 11$, thus, according to Eqs. 2 to 4, the real and imaginary SOM strengths for the two nuclei should be almost the same. This is essentially so for the real potential, as the volume–integral–per–nucleon for ^{89}Y is $J_v = 424.5$ MeV–fm^3, and that for ^{93}Nb is 426.3 MeV–fm^3 (see numerical potential values of Table 1). However, this is not true for the volume–integral–per–nucleon of the imaginary interaction, $J_w = 66.5$ MeV–fm^3 for ^{89}Y, but $J_w = 75.9$ MeV–fm^3 for ^{93}Nb.

Because of the above differences in J_w, a Zr SOM was sought which would fit the observed ^{89}Y/Zr and ^{93}Nb/Zr elastic–scattering ratios, in the following way: It was assumed that the ^{89}Y spin–orbit potential of Table 1 is appropriate for Zr, and that the real SOM potential strength for Zr can be obtained from that for ^{89}Y through the use of Eqs. 2 to 4. The $A^{1/3}$ size effect was taken into account, but the reduced geometric parameters were fixed to the ^{89}Y values of Table 1. The imaginary Zr potential was then varied to obtain the best fit to the observed ratio data, assuming the experimental values had equal weights. The usual $(N - Z)$ dependence of the imaginary strength was replaced by a dependence on ΔN, the number of neutrons (or neutron holes) outside the closed shell. Thus

$$W_0 = W + W_1 \cdot \Delta N. \tag{5}$$

Since ^{90}Zr and ^{96}Zr have similar low–lying level structures,[24] it is reasonable to assume that $N = 56$ has similar properties to the shell closure at $N = 50$, and that the six additional neutrons have filled the $d_{5/2}$ subshell. Thus, ΔN takes on the values 0, 1, 2, 2, and 0 for $A = 90$, 91, 92, 94, and 96, respectively. A best fit was obtained when the derivative Woods–Saxon imaginary potential had the values

$$\begin{aligned} W_0 &= (8.646 + 0.1 \cdot \Delta N) \text{ MeV} \\ r_w &= 1.293 \text{ fm} \\ a_w &= 0.428 \text{ fm}. \end{aligned} \tag{6}$$

The predicted $^{89}Y/Zr$ elastic–scattering ratios, shown in Fig. 9A, use this Zr potential together with the ^{89}Y potential parameters given in Table 1, whereas the $^{93}Nb/Zr$ ratios, shown in Fig. 9B, used the ^{93}Nb potential of Table 1 to calculate the numerator of the ratio. As is evident from these two figures, a reasonably satisfactory description of both ratios is obtained. Moreover, the Zr SOM radius is essentially the same as that of ^{93}Nb, the imaginary diffuseness is midway between that of yttrium and niobium, as is the elemental J_w deduced from the five Zr isotopes (J_w = 70.9 MeV–fm^3). From Eqs. 3 and 4, it follows that, for a derivative Woods–Saxon potential, the rate of change of J_w with respect to Z, with N held constant, is

$$\left.\frac{\partial J_w}{\partial Z}\right|_N = \frac{16\pi(14.94)}{A^2} R_w^2 a_w \left[1 + \frac{1}{3}(\pi a_w/R_w)^2\right]$$

$$= 1.3 \text{ MeV–fm}^3 , \qquad (7)$$

where $R_w = r_w \cdot A^{1/3}$, and the numerical value is relevant to ^{89}Y. (In Eq. 7, terms arising from $\partial A/\partial Z$ have been neglected, since, for conventional values of the SOM parameters, they change the numerical results by less than 5%.) Empirically, the value in this region is ΔJ_w = 4.2 MeV–fm^3, going from Z = 39 to Z = 40. Thus, the elastic–scattering ratios in the A ≈ 90 region are simply explained by the fact that the imaginary portion of the SOM is changing much more rapidly, as one moves away from the "doubly–magic" ^{88}Sr nucleus, than predicted by conventional "global" potentials (e.g., by that of Walter and Guss[5]).

B. Inelastic Neutron Scattering

As cited above, the present experiments did not distinguish between elastically–scattered and inelastically–scattered neutrons due to the excitation of the 320–keV (5/2$^-$) state[21] in ^{51}V. To this point, it has been assumed that any inelastic scattering is due to CN processes, resulting in inelastic–scattering cross sections that are negligibly small at the 8 MeV incident–neutron energies of the present work. On the other hand, there may be a significant direct inelastic–scattering component similar to that observed in the neighboring nucleus, ^{54}Fe, where the cross section for inelastic–neutron excitation of the 1.41 (2$^+$) state is ≈ 40 mb at an incident energy of 11 MeV.[32] In order to examine the effect of direct inelastic scattering on the measured $^{51}V/Cr$ ratios, it was assumed that the total cross section for the inelastic excitation of the 5/2$^-$ state in ^{51}V was also 40 mb. The associated angular distribution of the inelastically–scattered neutrons was calculated using the DWBA approximation and the computer code PTOLEMY.[33] In carrying out the calculation, the ^{51}V SOM of Table 1 was used (with no spin–orbit interaction) to calculate the distorted waves. The form factor of the transition potential was taken to be dU/dr, where U is the sum of the real and imaginary SOM interactions in ^{51}V. The resulting calculated inelastic–neutron angular distribution is shown in Fig. 10A.

The calculated inelastic–scattering cross sections for the excitation of the 5/2$^-$ state were subtracted from the observed ^{51}V cross section, shown in Fig. 1, and a new SOM was fitted to the resulting "elastic–scattering" distribution. In constructing this new potential, the ^{51}V spin–orbit interaction, r_v, and r_w were held fixed to the values of Table 1. This constraint prevented anomalous results from the fitting procedure. In this way "corrected" values of V_0, W_0, a_v and a_w were obtained. The ^{51}V cross section used to calculate the

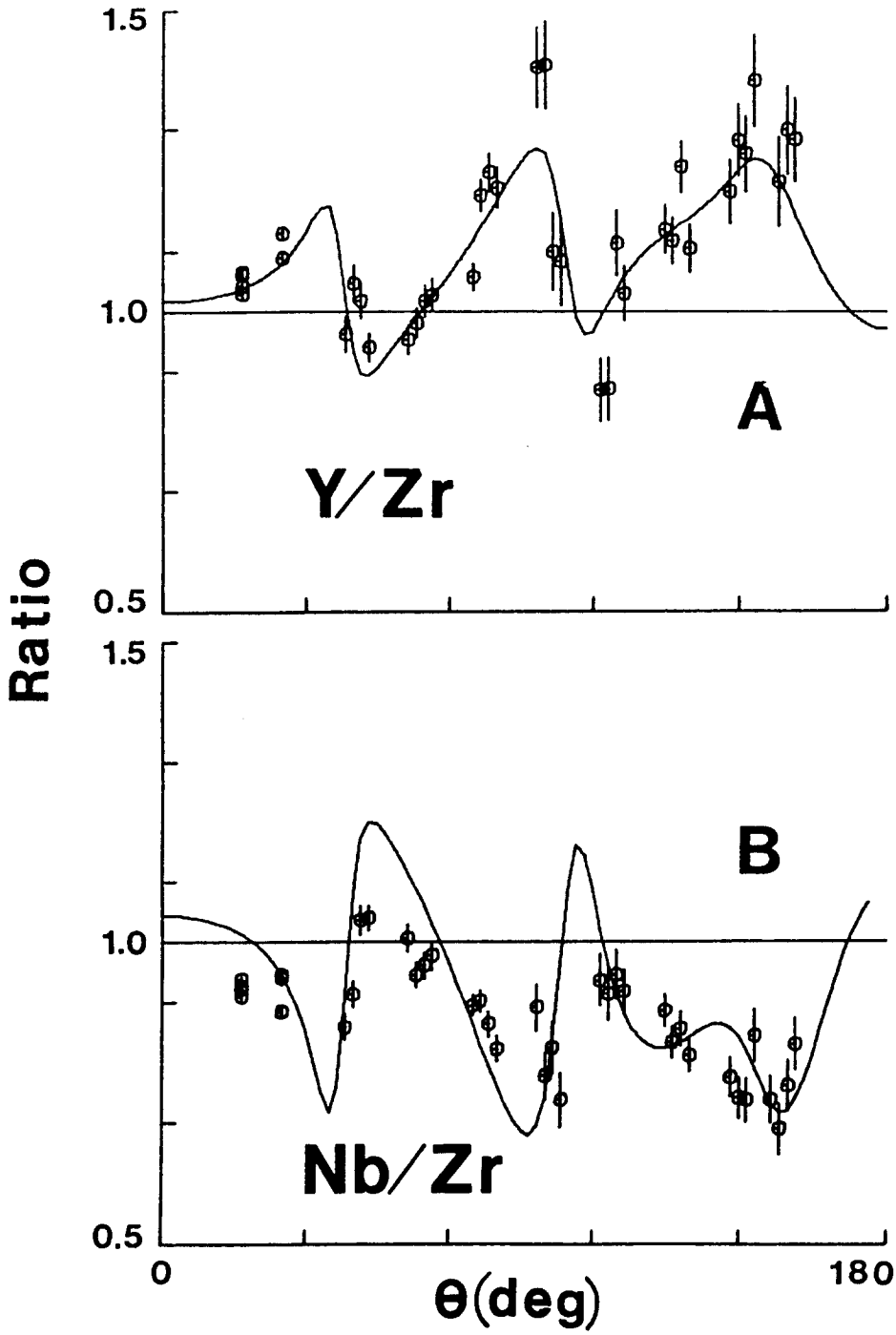

Fig. 9. Comparison of $^{89}Y/Zr(A)$ and $^{93}Nb/Zr(B)$ measured (data symbols) and calculated (curves) elastic–scattering ratios at an incident neutron energy of 8 MeV. The imaginary Zr potential is given by Eq. 6, and other details of the calculation are discussed in the text. The data are given in the laboratory coordinate system.

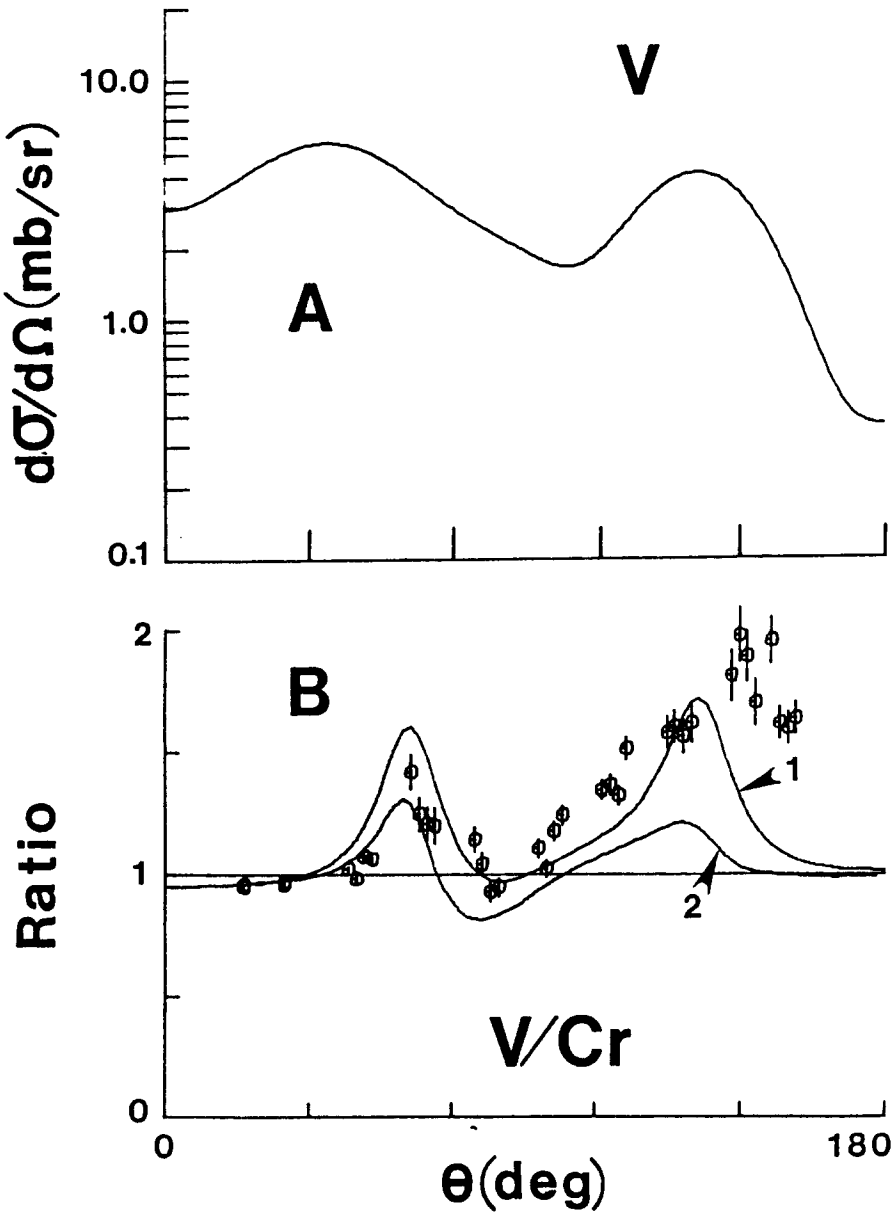

Fig. 10. Upper part "A", the differential cross section for the inelastic–neutron excitation of the 320 keV state in ^{51}V, calculated using the DWBA approximation and normalized to 40 mb, as described in the text. Lower part "B", a comparison of the measured and calculated ^{51}V/Cr elastic–scattering ratio. The measured values are indicated by "O" symbols. Curve "1" indicates the calculated result, including consideration of inelastic–neutron scattering, as described in the text. For comparison, curve "2" indicates the result calculated with the simple SOM described in Sec. III of the text, and shown in Fig. 1. The data are given in the laboratory coordinate system.

ratios was then computed using this "corrected" SOM, with the addition of the above direct inelastic contribution. The corresponding Cr cross sections for the isotopes making up the element were calculated using the same radii and diffusenesses, but with the strengths corrected for the isovector contributions as given by Eqs. 2 to 4. The resulting predicted elastic–scattering ratios are compared with the measured values in Fig. 10B. In this figure, the "1" curve indicates the result obtained as described above, while for comparison curve "2" indicates the results obtained using the conventional SOM discussed in Sec. III, and illustrated in Fig. 1.

It is evident that consideration of the direct–inelastic component distinctly improves the description of the observed quantities, particularly at angles $\leq 130^{o}$. The RMS deviation of the experimental values from the calculated results is 0.294 for curve "1", compared to 0.389 for curve "2". However, inelastic–neutron scattering alone does not account for the large experimentally–observed ratio values at scattering angles $> 130^{o}$. Since there appears to be no experimental knowledge of either the magnitude or angular distribution of the cross section for the inelastic–excitation of the first level in ^{51}V at 8 MeV incident–neutron energy, these considerations are at most qualitative. As shown in the next section, 40 mb is almost certainly too large a value for this cross section, and a better estimate would probably be in the 10–20 mb range. However, despite these uncertainties, one should be cautious of the measured ^{51}V/Cr elastic–scattering ratios, as they may have been significantly distorted by an inelastic–scattering contribution.

C. The Spin–spin Interaction

A term involving the scalar product of the intrinsic spin of the incident neutron, $\vec{\sigma}$, and the ground–state spin of the target nucleus, $\vec{I}$, can occur in the SOM. The magnitude of such a possible contribution was estimated following the procedure of Stamp.[34] If the residual nucleon–nucleon interaction has either a Bartlett or Majorana component, there is an additional term in the SOM of the form

$$V_s = \sum_i \vec{\sigma}\cdot\vec{\sigma}_i \, V(|\vec{r}-\vec{r}_i|), \tag{8}$$

where $\vec{\sigma}$ and $\vec{r}$ are the spin and spatial coordinates of the incident nucleon, and the sum on i is over all particles in the target. If we assume the spin of the target is carried by a few valence nucleons in the single–particle orbit j, moving outside a spin–zero core, the added term in the SOM due to the interaction of Eq. 8 can be written as

$$\begin{aligned} V_s &= \langle V(|\vec{r}-\vec{r}_i|)\rangle_i \frac{\langle\vec{\sigma}_i\cdot\vec{j}_i\rangle}{j(j+1)} \sum_i \vec{\sigma}\cdot\vec{j}_i \\ &= \langle V(|\vec{r}-\vec{r}_i|)\rangle_i \frac{\langle\vec{\sigma}_i\cdot\vec{j}_i\rangle}{j(j+1)} \vec{\sigma}\cdot\vec{I}, \end{aligned} \tag{9}$$

where

$$<V(|\vec{r}-\vec{r}_i|)>_i = \int |\Psi_i(\vec{r}_i)|^2 \, V(|\vec{r}-\vec{r}_i|) \, d\vec{r}_i \tag{10}$$

is the average over the wave function of the i^{th} target particle, and

$$<\vec{\sigma}_i \cdot \vec{j}_i> = j(j+1) - \ell(\ell+1) + \frac{3}{4} \tag{11}$$

is the expectation value of the projection of $\vec{\sigma}_i$ on the total spin, $\vec{j}_i$, of the i^{th} particle. In writing Eq. 9, it is clear that $\Sigma_i \vec{j}_i$ over all particles in the nucleus gives the total spin operator, $\vec{I}$, and, because of the assumption that the total nuclear spin is carried by the valence nucleons in a single–particle orbit, Eqs. 10 and 11 have the same value for each term contributing to the sum, and hence can be taken outside the summation sign of Eq. 9. Since the residual two–body interaction is attractive, $<V(|r-r_i|)>_i$ will generally be negative. However, the overall character of the spin–spin interaction is determined by the $<\vec{\sigma}_i \cdot \vec{j}_i>$ term of Eq. 9. According to Eq. 11, the spin–spin potential is attractive when the spin of the nucleus is carried by valence nucleons in a $j = \ell + 1/2$ orbit, and repulsive when the $j = \ell - 1/2$ orbit is involved.

In order to estimate the change in the predicted cross section due to the spin–spin term, the scattering problem can be solved in terms of the eigenfunctions of the operator

$$\vec{J} = \vec{I} + \frac{\vec{\sigma}}{2}, \tag{12}$$

where J can take on the values $I \pm 1/2$. In this representation, the expectation values of $\vec{\sigma} \, \vec{I}$ are

$$\begin{aligned} <\vec{\sigma}\cdot\vec{I}> \quad &= J(J+1) - I(I+1) - 3/4 = I \text{ (if } J=I+1/2) \\ &= -(I+1) \text{ (if } J=I-1/2). \end{aligned} \tag{13}$$

The SOM spin–orbit interaction, $\vec{\sigma}\cdot\vec{\ell}$, has off–diagonal matrix elements connecting these two possible J–states. However, if this coupling is neglected, the only effect of the added spin–spin interaction is to modify the usual real SOM by the addition of a term

$$V_s = <V(|r-r_i|)>_i \left[1 - \frac{\ell(\ell+1)-3/4}{j(j+1)}\right] \cdot \begin{bmatrix} I & (\text{if } J=I+1/2) \\ -(I+1) & (\text{if } J=I-1/2) \end{bmatrix}. \tag{14}$$

Therefore, if one solves, with a conventional SOM code, the scattering when $J=I+1/2$ and when $J=I-1/2$, the cross section can be obtained by combining the two components, multiplied by their statistical weights. Thus, in the limit that one neglects the coupling between $J=I+1/2$ and $J=I-1/2$ states induced by the spin–orbit potential, one obtains the result

$$\frac{d\sigma}{d\Omega} = \frac{1}{2(2I+1)}\left[(2I+2)\left(\frac{d\sigma}{d\Omega}\right)_{J=I+1/2} + 2I\left(\frac{d\sigma}{d\Omega}\right)_{J=I-1/2}\right], \tag{15}$$

where the factors multiplying the $\left(\frac{d\sigma}{d\Omega}\right)$ are the statistical weights, (2J+1), for the two possibilities.

In order to illustrate the effect, the specific case of the ^{59}Co/^{58}Ni elastic–scattering ratios is considered. In part, the reason for considering this ratio is that a detailed fit to the ^{58}Ni elastic–scattering data over the energy range 1.5 to 24 MeV has recently been carried out.[35] Thus we have a reliable 8 MeV SOM for ^{58}Ni, with the parameters given in Table 1. Following the conventional procedure of Sec. III, taking into account size and isovector effects (with the strengths of Eq. 4), one obtains curve "1" of Fig. 11, which is analogous to curve "1" of Fig. 2. In order to estimate the strength of the spin–spin interaction, it is assumed that the residual two–body force of Eq. 8 is given by the Schiffer–True potential.[36] A reasonable model for the ground state of ^{59}Co assumes the entire nuclear spin is carried by protons in the $0f_{7/2}$ shell. Thus, the interaction is between an incident neutron and a valence proton, so that one half the sum of the T = 0 and T = 1 Schiffer–True potentials should be used for V_s of Eq. 8. This interaction was averaged over the nuclear coordinates (Eq. 10) assuming the valence protons move in a harmonic oscillator well with $\hbar\omega = 41/A^{1/3} = 10.53$ MeV.[20] The resulting spin–spin potential of Eq. 14 was added to the ^{59}Co interaction for the two cases J = I+1/2 = 4 and J = I–1/2 = 3, with the results indicated by the calculated curves "2" and "3" of Fig. 11, respectively. In each instance, the spin–spin effect on the elastic–scattering ratio is small. The J = 4 case improves the agreement with the measured values near $\approx 60^{\circ}$, but is not as suitable in the 120° region. The situation is reversed for the J = 3 case. Consequently, when the two contributions are multiplied by their statistical weights and added together, Eq. 15, the net effect will be a negligible change in the predicted ratios. Although the mixing of the J = 3 and J = 4 states has been ignored in the above discussion, its inclusion is expected to give an effect no larger than that calculated from either of the individual J = 3 or 4 contributions.

It can further be seen that the addition of the spin–spin interaction produces a small change in the calculated ratios by evaluating the volume–integral–per–nucleon of the spin–spin potential strength, $\langle V(|r-r_i|)\rangle_i$ of Eq. 10,

$$\overline{V} = \frac{4\pi}{A}\int \langle V(|\vec{r}-\vec{r}_i|)\rangle\, r^2\, dr = 3.95 \text{ MeV–fm}^3 \tag{16}$$

Thus, $\overline{V}$ of the spin–spin interaction is less than 1% of the volume–integral–per–nucleon of the real ^{59}Co potential, $J_v = 454.4$ MeV–fm^3. The magnitude of $(A/4\pi)\overline{V}$, 18.56 MeV–fm^3, is similar to that found by Nagamine et al.,[37] who used other possible two–body interactions in their study of the polarization of neutrons scattered from ^{59}Co. Finally, Satchler[38] has pointed out that, because of the quenching of the M1 operator in nuclear–structure calculations,[20] the treatment of the spin–spin interaction in the above way probably sets an upper limit on the size of the effect. Thus, it is concluded that the addition of the spin–spin interaction to the SOM will not significantly change the calculated elastic–scattering ratios.

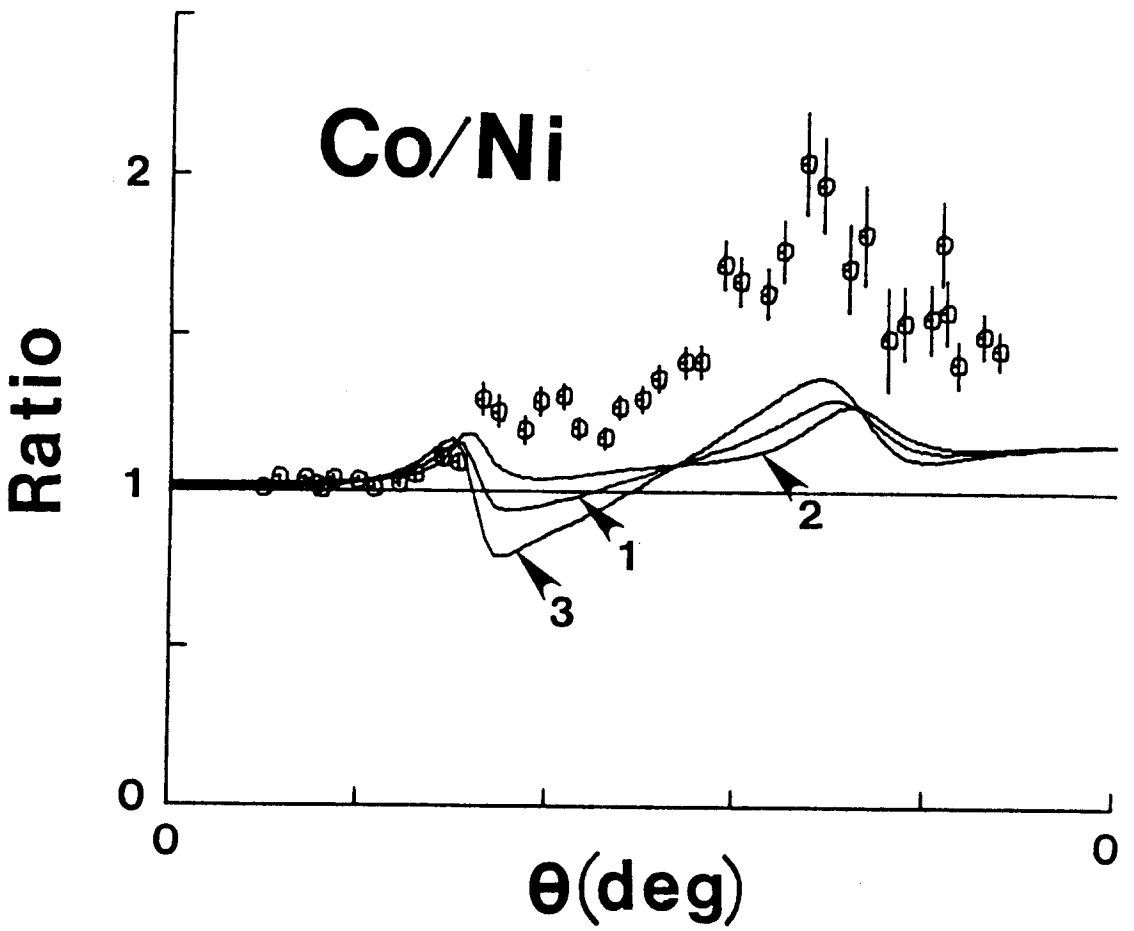

Fig. 11. The effect of the spin–spin interaction on the calculation of the $^{59}Co/^{58}Ni$ elastic–scattering ratio. The measured values are indicated by data symbols. Curve "1" represents the results of conventional SOM calculations, as described in Sec. III of the text. Curves "2" and "3" show the result of including the spin–spin interaction, with J = 4 and 3, respectively, as discussed in Sec. IV of the text. The data are given in the laboratory coordinate system.

D. The Effect of Deformation

From Table 1, it is clear that, in all cases, $r_w > r_v$, except for ^{58}Ni and ^{59}Co. Previously it has been found that when $r_v > r_w$, the nuclei tend to be deformed,[28] and that, at least in the $A \approx 60$ region, this decrease in r_w comes about when an SOM is used to describe a vibrational nucleus.[8] Furthermore, a satisfactory fit to ^{58}Ni neutron–scattering data over the energy range $\approx$ 1–24 MeV has been achieved using a vibrational model.[35] Thus, it is of interest to consider the effect of a vibrational model on the prediction of ^{59}Co/^{58}Ni elastic–scattering ratios.

A conventional ^{58}Ni vibrational model was used, coupling the ground state, the one–phonon level at 1.454 MeV (2^+), and the two–phonon triplet of levels at 2.942, 2.776, and 2.459 MeV, with spins of 0^+, 2^+, and 4^+, respectively.[23] A weak–coupling model was assumed for ^{59}Co consisting of an $f_{7/2}$ proton hole coupled to the ^{60}Ni ground state, the one–phonon 1.333 MeV (2^+) level, and the 0^+, 2^+, 4^+ two–phonon triplet at 2.285, 2.159, and 2.506 MeV, respectively.[39] With this model, the ^{59}Co neutron scattering is similar to that of ^{60}Ni, but modified to take into account the proton hole. Calculations using such a model can be carried out with the computer code PTOLEMY.[33] However, PTOLEMY does not treat the spin–orbit interaction when the nucleus is deformed, so the following approximate procedure was adopted:

i) A vibrational model for ^{58}Ni was obtained by fitting the 8 MeV elastic–scattering data using real Woods–Saxon and imaginary derivative Woods–Saxon wells, with $\beta_2 = 0.25$, and no spin–orbit interaction.

ii) The interaction between the incident neutron and the ^{60}Ni–plus–proton–hole configuration (the ^{59}Co nucleus) was assumed to have the same geometry as this ^{58}Ni potential, but with strengths modified according to Eqs. 2 to 4. Except for the channel coupling, this potential was used to describe neutron scattering from ^{59}Co.

iii) The potential which provides the coupling between the various channels in the scattering problem was assumed to have the same β_2 and geometry as for ^{58}Ni, but with strengths modified according to Eq. 2 to 4 so as to be applicable to ^{60}Ni.

With the above assumptions, the predicted ^{59}Co/^{58}Ni elastic–scattering ratio, given by the "1" curve of Fig. 12, was obtained. A comparison of this result with the "1" curve of Fig. 2, indicates that this vibrational model gives ratio results very similar to those obtained with the simple SOM. Thus, the effect of channel coupling is small, and this is consistent with the theorem, stated by Satchler,[40] which says that if the even A nucleus is a simple vibrator, and if its odd–A neighbor is described in terms of the weak–coupling model (i.e., no mixing of the various phonon states), then their elastic–scattering angular distributions will be identical, provided the SOMs used in the two cases are the same and that no $A^{1/3}$ size dependence is considered. That this is true for the vibrational model used in this case follows from the fact that if one neglects the isovector and $A^{1/3}$ variation of the SOMs and further assumes that the excitation energies of the one– and two–phonon states in ^{60}Ni are the same as in ^{58}Ni, then the scattering problem to be solved is the same for ^{59}Co and ^{58}Ni.

As pointed out by Satchler,[40] the even–odd elastic–scattering cross–section difference is much larger for rotational nuclei than for simple vibrators. Thus, it is

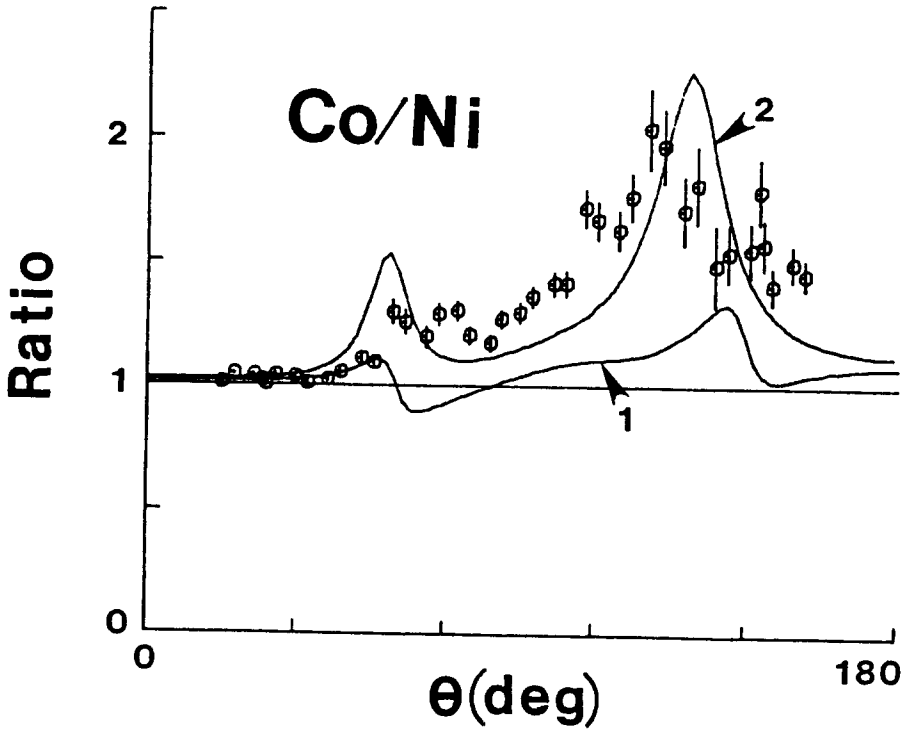

Fig. 12. Comparison of measured and calculated $^{59}Co/^{58}Ni$ elastic–scattering ratios. Experimental values are indicated by "O" symbols. Calculated results are indicated by curves where "1" corresponds to the vibrational model, and "2" to the rotational model, as described in the text. The data are given in the laboratory coordinate system.

instructive to examine the elastic–scattering–ratio predictions when ^{58}Ni and ^{59}Co are assumed to be rotational nuclei. This was done as follows.

It was assumed that ^{58}Ni is a rotational nucleus with $\beta_2 = 0.20$, and a fit to the 8 MeV neutron elastic–scattering data was carried out assuming that only the yrast 0^+, 2^+, and 4^+ levels[23] are coupled. The radii of the real and imaginary potentials were held fixed, as was the spin–orbit potential. The results of this fitting procedure, carried out with the computer code ANLECIS,[41] are given in Table 2. The isovector corrections to this potential, so as to make it appropriate for ^{59}Co, were made according to Eqs. 2 to 4, and the cross section for ^{59}Co was calculated assuming the $7/2^-$ ground state, the 1.190 MeV ($9/2^-$) and the 1.429 MeV ($11/2^-$) states form a rotational band. The ^{59}Co/^{58}Ni elastic–scattering ratios obtained with these assumptions are indicated by the "2" curve of Fig. 12, and are in reasonable agreement with the experimental results.

Table 2

Potential parameters obtained from fitting the ^{58}Ni neutron elastic–scattering distributions, assuming a rotational model, as described in the text.

Real Potential

V_o	=	48.262 MeV
r_v	=	1.2538 fm
a_v	=	0.6511 fm

Imaginary Potential

W_o	=	12.119 MeV
r_w	=	1.2538 fm
a_w	=	0.3477 fm

Spin–Orbit Potential

V_{so}	=	6.220 MeV
r_{so}	=	1.017 fm
a_{so}	=	0.600 fm

It is certainly true that ^{59}Co and ^{58}Ni are neither simple vibrators (i.e., instead of being degenerate, the two–phonon triplet in ^{58}Ni is split by 483 keV), nor rotational nuclei (i.e., the 0^+, 2^+, and 4^+ levels in ^{58}Ni and the $7/2^-$, $9/2^-$, and $11/2^-$ levels in ^{59}Co have

excitation energies quite different from those given by the I(I+1)–rule. However, as Hicks and McEllistrem[42] have pointed out, the large reorientation cross section that produces the odd–even difference need not necessarily imply a rotational model, but can merely reflect a strong coupling between the ground and one or several excited states, and this would seem to be the case for the $^{59}Co - ^{58}Ni$ pair.

E. Variation of the SOM Geometry

Except for some aspects of the treatment of the rapid variation of the imaginary potential near A ≈ 90, r_v, a_v, r_w, and a_w have been held fixed in the above discussion of the SOM for neighboring nuclei. In the following remarks, the constraint of fixed real and imaginary geometric parameters is removed, with the spin–orbit interaction remaining constant.

With the removal of the above constraints, a quite good description of the observed ^{51}V/Cr elastic–scattering ratios can be obtained using the SOM, as illustrated in Fig. 13A. In this prediction, inelastic–neutron excitation of the $5/2^-$ state in ^{51}V was assumed negligible, and the ^{51}V scattering was calculated using the potential of Table 1. The calculation of Cr elastic scattering used the same geometries for each isotope, adjusted to achieve the best description of the observed ratios. The resulting parameters are given in Table 3. A comparison of the values of Table 1 and Table 3 shows that the Cr r_v and r_w values are very nearly identical to those of ^{51}V, whereas a_v is ≈ 9% smaller and a_w ≈ 20% larger than those of the neighboring ^{51}V nucleus. The real isovector strength, 17.726 MeV,

Table 3

Chromium SOM parameters derived by fitting the observed ^{51}V/Cr elastic–scattering ratios, as described Section IV–E of the text.

Real Potential

$$V = (45.863 - 17.726\cdot(N-Z)/A\ )\ \text{MeV}$$

$$r_v = 1.2636\ \text{fm}$$

$$a_v = 0.5610\ \text{fm}$$

Imaginary Potential

$$W = (6.719 - 7.174\cdot(N-Z)/A)\ \text{MeV}$$

$$r_w = 1.2844\ \text{fm}$$

$$a_w = 0.5766\ \text{fm}$$

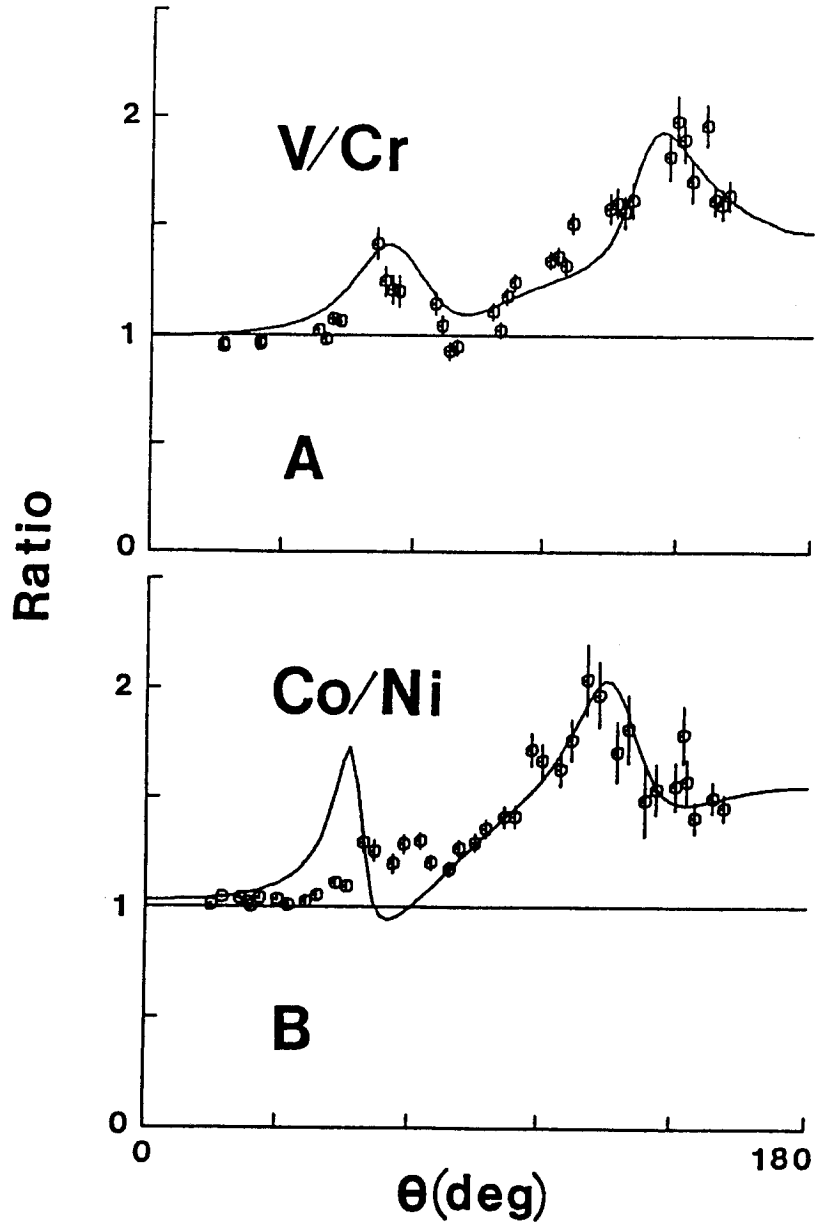

Fig 13 Upper portion "A", elastic–scattering $^{51}V/Cr$ ratio (curve) calculated using the ^{51}V potential of Table 1 and the Cr potential of Table 3, compared with the measured values (O symbols). Lower portion "B", elastic scattering $^{59}Co/^{58}Ni$ ratio calculated with the potentials of Table 1 (curve) compared with the measured values (O symbols). The details of the calculations are discussed in Sec. IV–E of the text. The data are given in the laboratory coordinate system.

is similar to that given in Eq. 4, but the imaginary isovector strength is only about half that of Eq. 4. Thus, the real potentials are quite similar, with J_v of the Cr potential being $\approx 2.7\%$ smaller than that of ^{51}V. On the other hand, the Cr $J_w = 82.65$ MeV–fm^3 is approximately 20% larger than that of the ^{51}V potential. From Tables 1 and 3, it follows that $\Delta J_w = 13.8$ MeV–fm^3 in going from Z = 23 to Z = 24, approximately four times the value given by Eq. 7 for nuclei in this mass region. This result is similar to the situation found near A ≈ 90, where the empirical value of $(\partial J_w/\partial Z)_N$ is about 3.25 times the value given by Eq. 7. Thus, in both the closed neutron–shell regions, N = 28 and N = 50, the rate of change of J_w with respect to Z, with N held constant, is considerably greater than generally predicted by global potentials (e.g., by that of Ref. 5).

The ^{58}Ni potential, given in Table 1, was obtained from a fit to measured elastic–scattering and total–cross–section data. The spin–orbit interaction was identical to that in ^{59}Co. The ratios obtained, when this interaction is combined with the ^{59}Co potential of Table 1, are compared with the experimental data in Fig. 13B. Aside from the neighborhood near ≈ 60°, the region of the first minima of the ^{59}Co and ^{58}Ni angular distributions, the predicted ratios are in good agreement with the measured values. As illustrated in Fig. 2, the first minima of these cross sections are very sharp. Thus the measured values are sensitive to small experimental perturbations (e.g., very small angular shifts) and to small imperfections in the SOM description which are magnified in the calculated cross–section ratios.

A comparison of the ^{59}Co and ^{58}Ni potentials given in Table 1 shows that the real radius, diffusenesses, and J_v values are very similar. The difference in J_v has a magnitude almost exactly equal to that given in the global model of Ref. 5. For the imaginary interaction, the radii and diffusenesses are within a few percent of each other, but the potential strengths differ by much more than predicted by the isovector contributions of Eqs. 3 and 4. Indeed, J_w for ^{58}Ni is about 22% larger than that for ^{59}Co, and ΔJ_w is about 2.5 times that predicted by the global SOM of Ref. 5. Thus again, the ratio data are consistent with neighboring odd–even pairs having real SOMs with similar geometries and strengths that are reasonably consistent with global values of the isovector potential, Eqs. 2 and 4. In contrast, the imaginary potential varies markedly between odd–even pairs, a behavior that is not well described by global models.

F. The Spin–Orbit Interaction

In the foregoing discussion, the spin–orbit interaction has remained fixed for a given pair. However, in the A ≈ 50–60 region, elastic scattering at large angles is particularly sensitive to the strength of this potential. If the variation of the strength of the spin–orbit potential is restricted to the global representation of Walter and Guss,[5]

$$
\begin{aligned}
V_{so} &= 2 \cdot V_{so}\, \vec{\sigma}\cdot\vec{\ell}\, \frac{1}{r}\frac{d}{dr}\frac{1}{(1+\exp((r-R_{so})/a_{so}))}, \\
V_{so} &= [(V_{so})_0 + 2\cdot((N-Z)/A)]\ \text{MeV}, \qquad (17) \\
R_{so} &= r_{so}A^{1/3}\ \text{fm},
\end{aligned}
$$

then the effect on the predicted elastic–scattering ratios is negligible. Furthermore, there appears to be no evidence from the ratio data at 8 MeV for the existence of an imaginary spin–orbit interaction.

On the other hand, when one relaxes the isovector constraints implied by Eq. 17, a substantial change in the predicted ratios can be obtained. If the ^{51}V potential, given in Table 1, is corrected according the Eqs. 2 to 4 so as to be applicable to the Cr isotopes, curve "1" of Fig. 14A is obtained, and it is identical to the "1" curve of Fig. 1. When the real and imaginary potentials are held constant and the spin–orbit potential for Cr is varied, considerably different ratios can be obtained. Curve "2" in Fig. 14A was calculated with a spin–orbit potential of

$$\begin{aligned} V_{so} &= 6.263 \text{ MeV}, \\ r_{so} &= 0.8337 \text{ fm}, \\ a_{so} &= 0.65 \text{ fm}. \end{aligned} \tag{18}$$

Near 80°, curve "2" provides somewhat inferior agreement with the observations and the structure at ≈ 120° is not evident in the measured values, but in the ≈ 140° range a markedly improved description of the observed values is obtained compared to that where the spin–orbit potentials of both elements of the pair are taken to be the same. Quantitatively, the RMS deviation of the calculated results from the measured values drops from 0.389 to 0.212.

A similar result is obtained for the ^{59}Co/^{58}Ni elastic–scattering ratios. Modifying the ^{59}Co potential of Table 1 with the isovector potential to make it applicable to ^{58}Ni, the predicted ratios shown by curve "1" in Fig. 14B are obtained (this is identical to curve "1" of Fig. 2). When the spin–orbit potential for ^{58}Ni is changed to

$$\begin{aligned} V_{so} &= 3.679 \text{ MeV}, \\ r_{so} &= 0.9045 \text{ fm}, \\ a_{so} &= 0.65 \text{ fm}, \end{aligned} \tag{19}$$

the predicted values of curve "2" of Fig. 14B are obtained. The RMS deviation of the experimental from calculated values is reduced from 0.360 to 0.299, but again the calculated result does not approach the measured values from ≈ 90° to 140°.

In the above calculations, all three parameters of the spin–orbit potentials for the Cr isotopes and ^{58}Ni were allowed to vary. For both cases, V_{so} and r_{so} for the even isotopes are smaller than the values for their odd–A neighbors. However, from the ratio data alone, there is no indication that the diffuseness changes between the neighboring ^{51}V/Cr and ^{59}Co/^{58}Ni pairs. This is not surprising, since the strength of the interaction, measured by its volume integral, J_{so}, is independent, in the first order, of a_{so},[43]

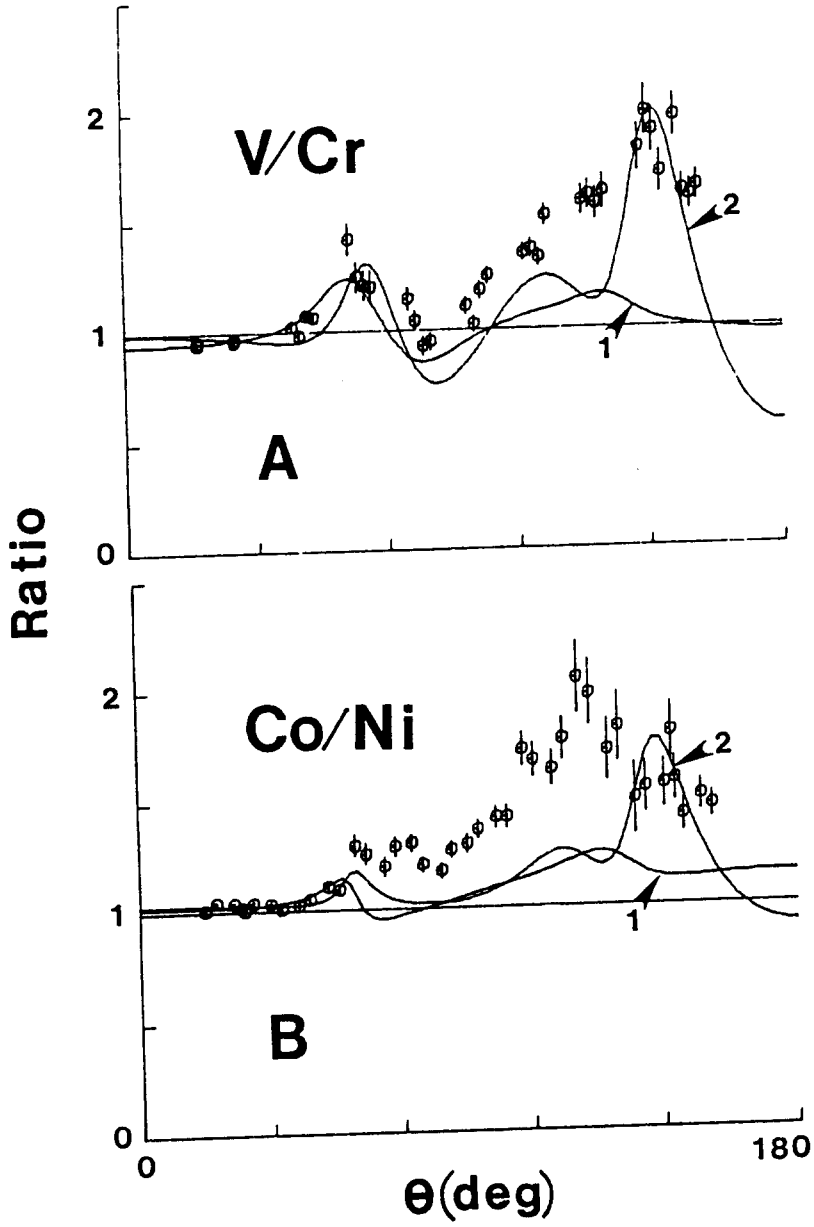

Fig. 14. Comparison of measured elastic–scattering ratios with the calculated predictions obtained by varying the spin–orbit potential. Upper part "A" refers to the $^{51}V/Cr$ ratio with curve "1" indicating the result of a conventional SOM calculation (identical to curve "1" of Fig. 1), and curve "2" that obtained by varying the spin–orbit potential as described in Sec. IV–F of the text. The experimental values are indicated by "O" symbols. Lower part "B" refers to the $^{59}Co/^{58}Ni$ ratio, with identical notation. The data are given in the laboratory coordinate system.

$$J_{so} = 2 \cdot V_{so} \int_0^{\infty} \frac{1}{r} \left[\frac{d}{dr} \frac{1}{(1+\exp((r-R_{so})/a_{so}))} \right] r^2 \, dr$$

$$= 2 \cdot V_{so} \, a_{so} \, \ln(1+\exp(R_{so}/a_{so}))$$

$$\approx 2 \cdot V_{so} \, R_{so} \, . \qquad (20)$$

Thus, in the A = 50–60 region, the calculated ratio results are quite sensitive to the spin–orbit potential, and in each case, the ratio data is better fitted if J_{so} for the even–A nucleus is about 60% of the value for the odd–A member of the pair (since elemental Cr is more than 90% even–A isotopes, it can be reasonably considered an even–A target). However, only when detailed polarization measurements are made will it be possible to assess whether or not the spin–orbit potential is appreciably different for neighboring odd and even nuclei.

V. DISCUSSION AND SUMMARY

In Sec. III it was shown that the 8 MeV elastic–scattering ratios for Cu/Zn, In/Cd and ^{209}Bi/Pb were fairly consistent with the predictions of regional SOMs, which include simple size and isovector contributions. For the In/Cd and ^{209}Bi/Pb elastic–scattering ratios, the isovector strengths were consistent with those of the global model of Walter and Guss[5] (Eq. 4). For the Cu/Zn ratio, the regional Fe and Cu potentials of El–Kadi et al.[6] were used. In that case the isovector real potential was very similar to that of Eq. 4 (15.3 MeV and 15.85 MeV, respectively). On the other hand, the isovector imaginary strength of Ref. 6 is 1.6 times the 14.94 MeV suggested in Ref. 5 (and given in Eq. 4). All three of these ratios have the common characteristic that one member of the ratio has an appreciable mixture of several isotopes in the natural target used in the present measurements (i.e., two in Cu and In, five in Zn, seven in Cd and four in Pb). Thus, any variation in the SOM geometry between isotopes would tend to average out, and this may contribute to the success of the constant–geometry regional models in describing these three ratios.

The most successful SOM description is obtained in the case of the heaviest pair, ^{209}Bi/Pb. These nuclei are near the doubly–closed Z = 82, N = 126 shell and, consequently, show little tendency to be deformed. In the other two "regional successes", theory and experiment show some deviation from one another in the $\approx 130^{\circ}$–150° angular region. In both cases this is near the back–angle minimum, where the elastic–scattering cross sections are quite small (e.g., $d\sigma/d\Omega \approx 7$ mb/sr). If an inelastic–scattering contribution of only 1–2 mb/sr were added to the Cu and Cd elastically–scattered components, theory and experiment would be in good agreement. In both of these latter cases there is some concern that the experimental measurements did not fully resolve the elastically–scattered component from inelastically–scattered contributions due to the excitation of low–lying levels in Cu and Cd isotopes. The observed cross section for the inelastic–neutron excitation of the yrast 2^+ level of ^{54}Fe (Ref. 32) is ≈ 2 mb/sr, and a similar magnitude for the even Cd isotopes is not unreasonable. On the other hand, for the Cu isotopes, unresolved inelastic scattering involves the excitation of $1/2^-$ states at ≈ 700 keV.[24] These states are well described by the weak coupling model[20] in which a $p_{3/2}$

proton couples to the first 2^+ level in ^{62}Ni or ^{64}Ni to give a quartet of states in ^{63}Cu and ^{65}Cu, respectively. The lowest members of these quartets are the $\approx$ 700 keV $1/2^-$ states. With this model, inelastic–neutron scattering to the $1/2^-$ state is expected to be 1/10 the magnitude of the ^{62}Ni or ^{64}Ni excitation (i.e., have a magnitude of $\approx$ 0.2 mb/sr). Thus, if one takes seriously the small deviation between theory and experiment for the Cu/Zn ratios in the $\approx 130^o$ to 150^o angular range, one may have to make some minor changes in the constant–geometry regional model.

It is well known that, in the region of A $\approx$ 90, the imaginary portion of the SOM is rapidly changing.[28] From detailed fits to elastic–scattering data for ^{89}Y and ^{93}Nb (Refs. 9 and 10, respectively), this is not so much a change in well depth or radius of the imaginary interaction, but rather is due to a rapidly changing imaginary diffuseness in this mass region (i.e., a_w for ^{93}Nb is $\approx$ 20% larger than that of ^{89}Y). The ^{89}Y/Zr and ^{93}Nb/Zr ratio data lead to the same conclusion—the main difference between the 8 MeV Zr SOM and those for ^{89}Y and ^{93}Nb is in the diffuseness of the imaginary interaction. If one makes a Taylor's–series expansion of J_w about the value for ^{89}Y, one obtains the expression

$$J_w = (66.47 + 4.17 \cdot \Delta Z + 0.54 \cdot \Delta N) \quad \text{MeV–fm}^3 , \tag{21}$$

where $\Delta Z = Z - 39$, $\Delta N = N - 50$, and J_w is the volume integral–per–nucleon of the imaginary potential for the nucleus with $Z = 39 + \Delta Z$ and $N = 50 + \Delta N$. The constants in Eq. 21 were evaluated using the ^{89}Y, ^{93}Nb, and ^{90}Zr J_w values obtained from the SOM parameters given in Table 1 and Eq. 6. Thus, in this limited mass region, the rate of change of J_w depends much more strongly on ΔZ than on ΔN. This is consistent with a shell–model description of nuclei in this mass region, since the number of low–lying excited states increases much more rapidly as one adds protons to the $(p_{1/2},g_{9/2})$ configuration outside the Z = 38, N = 50 closed shell, than when one adds neutrons which go predominantly into the $d_{5/2}$ orbit.

Thus, a regional SOM near A $\approx$ 90 seems to be one in which the real potential has fairly constant geometrical parameters and an isovector strength consistent with that suggested by Walter and Guss[5] (Eqs. 2 and 4). However, the imaginary interaction is quite different from that usually suggested—it has a fairly constant well depth but a rapidly increasing diffuseness as one goes away from the Z = 38, N = 50 doubly–closed shell.

The remaining two cases (^{51}V/Cr and ^{59}Co/^{58}Ni), where the simple size and isovector predictions do not fit the data, involve relatively light nuclei. In these cases, fluctuations, even at the relatively–high 8 MeV energy, may bring into question the use of the SOM. Be that as it may, in both instances, the agreement between theory and experiment is markedly improved if the well depth and radius of the spin–orbit interaction are both reduced in the denominator of each ratio. Since natural Cr has $\approx$ 90% even–isotope abundance, this implies that the spin–orbit strength for the even–A member of these two ratios is weaker than that for its odd–A neighbor. In both cases, the experiments are consistent with the even–A spin–orbit strength being only about 60% of that of its odd–A neighbor, where the strength is measured by the radial integral of the Thomas term, J_{so}, given by Eq. 20. Since there are other ways of predicting the experimentally–observed ratios, these considerations do not necessarily imply a reduction in the spin–orbit strength. Whether or not this reduction exists can only be tested when detailed polarization measurements are carried out and analyzed in this mass region.

For nuclei in the A = 50–60 region, reasonable agreement with the ratio data can also be obtained if one relaxes the equal–geometry criterion for neighboring pairs. With the possible exception of the $^{51}V - Cr$ pair, which shows a 9% difference in a_v, all the ratios measured in the present work are consistent with an essentially constant–geometry regional SOM for the real potential, with isovector strength variations more or less consistent with Eq. 4. (It should be noted that the Cr SOM given in Table 3 was deduced assuming the spin–orbit interaction of Cr and ^{51}V were the same, and ignoring any possible inelastic excitation of the $5/2^-$ level in ^{51}V. If these two effects were included in the fit, one might find that the 9% difference in a_v between the pair would vanish.) Variations in the geometry between neighboring pairs is, of course, expected, since the real SOM satisfies the dispersion relationship[44]

$$V(r,E) = V_{HF}(r,E) + \frac{P}{\pi}\int_{-\infty}^{\infty} \frac{W(r,E')}{E-E'}\,dE' \,, \qquad (22)$$

where V(r,E) is the total real SOM interaction, $V_{HF}(r,E)$ is its Hartree–Fock component, P denotes the principal–value integral, and W(r,E) is the absorption potential. Since, at the energies of interest here, W(r,E) is surface peaked, one would expect the principal–value integral to change mainly the surface characteristics of the real potential. If one characterizes V(r,E) in terms of its radial moments,[45] $\langle r^q \rangle$, then for ^{51}V at 8 MeV, the principal value integral for q = 0.8, 2 and 4 contributes[7] only 4.9%, 6.6%, and 8.4%, respectively, to the q^{th} moment of the total potential. Thus, since variations in the geometry of the real potential between neighboring nuclei are mainly due to differences of these small contributions, one would expect r_v and a_v for the particular pair to be quite similar, and the ratio results are consistent with this expectation.

Turning to the imaginary potential, the strength, J_w, in the A = 50–60 region shows a rapid increase going from ^{51}V to Cr and from ^{59}Co to ^{58}Ni. As can be seen from Tables 1 and 3 for the ^{51}V–Cr pair, there is little difference in W_0 and r_w, and almost the entire increase in J_w is due to the fact that a_w of Cr is $\approx$ 19% larger than for ^{51}V. Thus, the situation here is nearly identical to that found near A $\approx$ 90. On the other hand, Table 1 shows that the value of a_w for ^{58}Ni is only about 6% larger than that for ^{59}Co, while the increase in W_0 is more than twice the 0.75 MeV predicted by Eqs. 3 and 4. Thus the situation is quite different from that previously encountered, and perhaps this difference implies that the SOM is not appropriate in this mass–energy range. In an earlier study at this laboratory,[8] it was found that the imaginary potential of the SOM for ^{59}Co decreased with energy, and, in contrast to most spherical nuclei, r_v was greater than r_w. It was shown[8] that these trends will emerge if one attempts to fit data from a vibrational nucleus with an SOM. Thus, the ^{59}Co and ^{58}Ni nuclei may be deformed. In Sec. IV it was shown that if a rotational model is used for both ^{59}Co and ^{58}Ni, the agreement between measured and calculated elastic–scattering ratios was very much improved. As pointed out by Hicks and McEllistrem,[42] the large reorientation effect, which leads to the differences between the ^{59}Co and ^{58}Ni cross sections, does not necessarily imply that the nuclei are rotational, but does indicate a strong coupling between the ground and one or more excited states. It is probably this latter effect that is contributing to the observed $^{59}Co/^{58}Ni$ elastic–scattering ratios.

As was already mentioned, neutrons resulting from the excitation of the 320 keV level in ^{51}V were not resolved from the elastically–scattered contribution in the present

experiments. In Sec. IV, the possible effect of this inelastically–scattered component on the predictions of the ^{51}V/Cr ratios was examined. It was concluded that the effect might be significant but could not fully account for the differences between the measured and calculated elastic–scattering ratios. Furthermore, those estimates of the inelastic–scattering contributions are probably an upper limit because of the following considerations. The N = 28 isotones (^{50}Ti, ^{51}V, ^{52}Cr, ^{53}Mn, and ^{54}Fe) have low–lying spectra that are well described by considering the valence protons to be filling the $f_{7/2}$ shell outside an inert ^{48}Ca core.[20] On the basis of this model, the E2 γ–decay of the ^{51}V 5/2$^-$ level and the ^{54}Fe yrast 2$^+$ level are described by the $(\pi f_{7/2})^3_{5/2^-} \rightarrow (\pi f_{7/2})^3_{7/2^-}$ and $(\pi f_{7/2})^6_{2^+} \rightarrow (\pi f_{7/2})^6_{0^+}$ transitions, respectively. From these assumptions, it follows that the ratio of the B(E2)s governing these γ–decays should be

$$\frac{B(E2;\ 5/2^- \rightarrow 7/2^-)}{B(E2;\ 2^+ \rightarrow 0^+)} = 16/9 = 1.78\ . \qquad (23)$$

Experimentally, B(E2) in ^{51}V is[46] 154 e^{2}fm^4, and in ^{54}Fe is[47] 128 e^{2}fm^4, so the ratio is 1.2. Thus the E2 γ–decay in ^{54}Fe is much more enhanced than in ^{51}V. Although the degree of enhancement in neutron scattering is not necessarily the same as for γ–decay, the same general trend is to be expected. Thus a more realistic estimate of the total direct inelastic scattering cross section for the 5/2$^-$ level in ^{51}V is probably 10–20 mb, rather than the 40 mb used in the discussion of the preceding Section.

The effect of a possible spin–spin interaction was examined, where the magnitude and radial form were deduced on the assumption that the Schiffer–True potential[36] describes the force between the incident neutron and the valence nucleons. A method for approximately calculating the effect of this $\vec{\sigma}\cdot\vec{I}$ interaction (where $\vec{\sigma}$ and $\vec{I}$ are the spins of the incident neutron and target nucleus, respectively) using conventional SOM codes was given. It was concluded that the spin–spin interaction has a negligible effect on the elastic scattering of the odd–A member of a given pair and, consequently, is not a factor in explaining the elastic–scattering ratio data.

Finally, it should be emphasized that the above measurements and their interpretation demonstrate that global SOMs are suitable for no more than a qualitative description of many physical observables. Regional SOMs are far more appropriate for quantitative results, but even they have significant shortcomings in many applications, as the potential can change very rapidly with target mass, and particularly with target Z near shell closures. These changes reflect fundamental structural differences in the targets that will be most evident at relatively low (e.g., few–MeV) energies, and cannot be avoided. As one goes to higher energies, one would expect the structure differences to become less important, and the concept of the regional SOM to be more valid. Evidence that this may be true comes from the data of Ref. 48, where the measured ^{59}Co/Ni ratio at 21.6 MeV appears consistent with a regional SOM interpretation, and does not show the large deviations from unity observed in the present, and lower–energy, measurements. The present work implies that detailed SOMs necessary for the quantitative provision of a number of aspects of data for applied purposes (e.g., the provision of transmission coefficients used in calculating neutron–emission spectra) must be based upon comprehensive measured data, carefully interpreted, for the particular targets of interest.

ACKNOWLEDGMENTS

The authors are indebted to Dr. S. C. Pieper for several helpful discussions.

REFERENCES

1. P. E. Hodgson, Nuclear Reactions and Nuclear Structure Clarendon Press, Oxford (1971).

2. D. Wilmore and P. E. Hodgson, Nucl. Phys. 55 673 (1962).

3. F. Becchetti and G. Greenlees, Phys. Rev. 182 1190 (1969).

4. J. Rapaport, Phys. Reports 87 25 (1982).

5. R. L. Walter and P. P. Guss, Proc. Inter. Conf. on Nucl. Data for Basic and Applied Purposes, P. Young et al., eds., Gordon and Breach, New York (1986).

6. S. M. El–Kadi, C. E. Nelson, F. O. Purser, R. L. Walter, A Beyerle, C. R. Gould and L. W. Seagondollar, Nucl. Phys. A390 509 (1982).

7. R. D. Lawson, P. T. Guenther and A. B. Smith, Nucl. Phys. A493 267 (1989).

8. A. B. Smith, P. T. Guenther and R. D. Lawson, Nucl. Phys. A483 50 (1988).

9. R. D. Lawson, P. T. Guenther and A. B. Smith, Phys. Rev. C34 1599 (1986).

10. A. B. Smith, P. T. Guenther and R. D. Lawson, Nucl. Phys. A455 344 (1986).

11. A. B. Smith, S. Chiba, P. T. Guenther and R. D. Lawson, to be published.

12. R. D. Lawson, P. T. Guenther and A. B. Smith, Phys. Rev. C36 1298 (1987).

13. A. M. Lane, Phys. Rev. Lett. 8 171 (1962).

14. A. Smith, P. Guenther, R. Larson, C. Nelson, P. Walker and J. Whalen, Nucl. Instr. Meth. 50 277 (1967).

15. A. B. Smith, MONTE–SPHERE, A Monte–Carlo multiple–event correction code (1988), unpublished.

16. C. Budtz–Jorgensen, P. Guenther, A. Smith, J. Whalen, W. McMurray, M. Renan and I. Van Heerden, Z. Phys. A319 47 (1984).

17. A. Smith, P. Guenther, J. Whalen, I. Van Heerden and W. McMurray, J. Phys. G11 125 (1985).

18. P. Guenther, A. Smith and J. Whalen, Phys. Rev. C12 1797 (1976).

19. Chart of the Nuclides Knolls Atomic Power Laboratory, 13th Edition (1983).

20. R. D. Lawson, Theory of the Nuclear Shell Model Clarendon Press, Oxford (1980).

21. C. Zhou, E. Zhou, X. Lu and J. Hou, Nucl. Data Sheets 48 111 (1986).

22. P. Anderson, L. Ekstrom and J. Lyttkens, Nucl. Data Sheets 39 641 (1983).

23. L. K. Peker, Nucl Data Sheets 42 457 (1984).

24. C. M. Lederer and V. S. Shirley, eds., Table of Isotopes, 7th Edition, John Wiley and Sons, New York (1978).

25. J. Blachot and G. Marguier, Nucl. Data Sheets 52 565 (1987).

26. R. D. Lawson and J. L. Uretsky, Phys. Rev. 108 1300 (1957).

27. A. B. Smith and P. T. Guenther, to be published.

28. A. Smith, P. Guenther and J. Whalen, Nucl. Phys. A415 1 (1984).

29. A. Lane, J. Lynn, E. Melkonian and E. Rae, Phys. Rev. Lett. 2 424 (1959).

30. W. Vonach, A. Smith and P. Moldauer, Phys. Lett. 11 331 (1964).

31. S. Cohen, R. D. Lawson, M. H. Macfarlane and M. Soga, Phys. Lett. 10 195 (1964).

32. S. Mellema, R. W. Finlay and F. S. Dietrich, Phys. Rev. C33 481 (1986).

33. M. H. Macfarlane and S. C. Pieper, Argonne National Laboratory Report, ANL–76–11 (1978).

34. A. P. Stamp, Phys. Rev. 153 1052 (1967).

35. A. B. Smith et al., to be published.

36. J. P. Schiffer and W. W. True, Rev. Mod. Phys. 48 191 (1976).

37. K. Nagamine, A. Uchida and S. Kobayashi, Nucl. Phys. A145 203 (1970).

38. G. R. Satchler, Phys. Lett. B34 37 (1971).

39. P. Anderson, L. P. Ekstrom and J. Lyttkens, Nucl. Data Sheets 48 251 (1986).

40. G. R. Satchler, Nucl. Phys. 45 197 (1963).

41. P. A. Moldauer and J. Raynal, private communication (1983).

42. S. E. Hicks and M. T. McEllistrem, Nucl. Phys. A468 372 (1987).

43. S. G. Cooper and P. E. Hodgson, J. Phys. G6 L21 (1980).

44. G. R. Satchler Direct Nuclear Reactions Clarendon Press, Oxford (1983).

45. C. Mahaux and R. Sartor, Phys. Rev. Lett 57 3015 (1986).

46. R. Horoshko, D. Cline and P. M. S. Lesser, Nucl. Phys. A149 562 (1970).

47. Wang Gongquing, Zhu Jiabi and Zhang Jingen, Nucl. Data Sheets 50 255 (1987).

48. E. Ramstrom, private communication (1989); see also, N. Olsson, E. Ramstrom, B. Trostell and B. Holmqvist, Nuclear Energy Agency Report, NEANDC–222'U' (1985).